AD-A085 578 LOCKHEED MISSILES AND SPACE CO INC PALO ALTO CA PALO --ETC F/6 4/1
GROUND-BASED PHOTOMETRIC MEASUREMENTS HAES PROGRAM SUPPORT.(U)
JAN 79 R D SEARS DNA001-77-C-0329

UNCLASSIFIED DNA-4975Z NL

1 OF 2
AD A
085 578

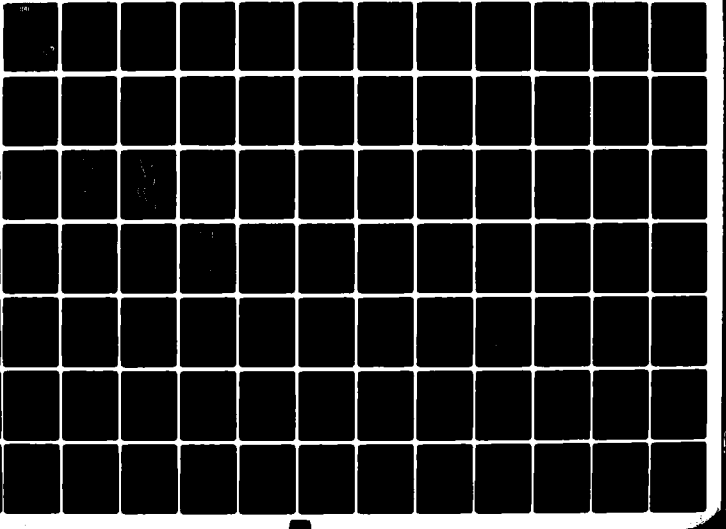

LEVEL III

DNA 4975Z

GROUND-BASED PHOTOMETRIC MEASUREMENTS

HAES Program Support

Lockheed Missiles and Space Co., Inc.
3251 Hanover Street
Palo Alto, California 94304

31 January 1979

Interim Report for Period 12 September 1977—31 January 1979

CONTRACT No. DNA 001-77-C-0329

THIS WORK SPONSORED BY THE DEFENSE NUCLEAR AGENCY
UNDER RDT&E RMSS CODE B322078462 I25AAXHX63278 H2590D.

Prepared for
Director
DEFENSE NUCLEAR AGENCY
Washington, D. C. 20305

Destroy this report when it is no longer needed. Do not return to sender.

PLEASE NOTIFY THE DEFENSE NUCLEAR AGENCY, ATTN: STTI, WASHINGTON, D.C. 20305, IF YOUR ADDRESS IS INCORRECT, IF YOU WISH TO BE DELETED FROM THE DISTRIBUTION LIST, OR IF THE ADDRESSEE IS NO LONGER EMPLOYED BY YOUR ORGANIZATION.

UNCLASSIFIED

SECURITY CLASSIFICATION OF THIS PAGE (When Data Entered)

REPORT DOCUMENTATION PAGE	READ INSTRUCTIONS BEFORE COMPLETING FORM
1. REPORT NUMBER: DNA 4975Z	2. GOVT ACCESSION NO.: AD-A085578
3. RECIPIENT'S CATALOG NUMBER:	
4. TITLE (and Subtitle): GROUND-BASED PHOTOMETRIC MEASUREMENTS HAES Program Support	5. TYPE OF REPORT & PERIOD COVERED: Interim Report for Period 12 Sep 77—31 Jan 79
	6. PERFORMING ORG. REPORT NUMBER:
7. AUTHOR(s): R. D. Sears	8. CONTRACT OR GRANT NUMBER(s): DNA 001-77-C-0329
9. PERFORMING ORGANIZATION NAME AND ADDRESS: Lockheed Missiles and Space Co., Inc. 3251 Hanover Street Palo Alto, California 94304	10. PROGRAM ELEMENT, PROJECT, TASK AREA & WORK UNIT NUMBERS: Subtask I25AAXHX632-78
11. CONTROLLING OFFICE NAME AND ADDRESS: Director Defense Nuclear Agency Washington, D.C. 20305	12. REPORT DATE: 31 January 1979
	13. NUMBER OF PAGES: 104
14. MONITORING AGENCY NAME & ADDRESS(if different from Controlling Office):	15. SECURITY CLASS (of this report): UNCLASSIFIED
	15a. DECLASSIFICATION/DOWNGRADING SCHEDULE:

16. DISTRIBUTION STATEMENT (of this Report)

Approved for public release; distribution unlimited.

17. DISTRIBUTION STATEMENT (of the abstract entered in Block 20, if different from Report)

18. SUPPLEMENTARY NOTES

This work sponsored by the Defense Nuclear Agency under RDT&E RMSS Code B322078462 I25AAXHX63278 H2590D.

19. KEY WORDS (Continue on reverse side if necessary and identify by block number)

Aurora
Airglow
Photometer
Auroral Structure
Atmospheric Radiance

20. ABSTRACT (Continue on reverse side if necessary and identify by block number)

Ground-based photometric measurements of auroral and airglow intensities, motions, and spatial and temporal PSD's (power spectral densities) were made at Chatanika, Alaska in support of DNA/AFGL rocket and satellite experiments during the interval September 1977 through January 1979. The latitudinal variations of auroral, airglow, and ionospheric parameters were monitored using a multicolor, meridional scanning photometer. Horizontal motions and scale sizes were monitored using two multiple beam photometers. Data obtained in support of four DNA/AFGL rocket experiments, Field Widened Interferometer,

DD FORM 1 JAN 73 1473 EDITION OF 1 NOV 65 IS OBSOLETE

UNCLASSIFIED

SECURITY CLASSIFICATION OF THIS PAGE (When Data Entered)

20. ABSTRACT (Continued)

WIDEBAND Multi, SWIR/SWIR/TMA, and EXCEDE II, are presented herein. Data synopsis sheets describing the data obtained for a number of WIDEBAND satellite passes are also included.

PREFACE

This is the interim technical report on contract DNA 001-77-C-0329 covering the period 12 September 1977 through 31 December 1978. The purposes of the research conducted under this contract were to provide ground-based photometric support for a variety of DNA/AFGL infrared rocket experiments conducted under the HAES (High Altitude Effects Simulation) Program and to measure the spatial and temporal structure of auroral emission and of OH emission in the visible and near-infrared regions utilizing a newly developed MTP (Multibeam Telescopic Photometer).

The experimental and analytical efforts were conducted at the Lockheed Palo Alto Research Laboratory and at the LMSC optical field site at Chatanika, Alaska. The principal investigator on this program was Mr. R. D. Sears. Also contributing significantly to the program were D. R. Hillendahl and G. Rogers. We acknowledge the support and assistance of the SRI International personnel at the Chatanika field site, and of Dr. M. Baron and Dr. R. Vondrak of SRI International who contributed greatly to our cooperative programs involving the incoherent scatter radar and photometers. The support and encouragement of our DNA contract officer, Major J. Mayo, is gratefully acknowledged.

CONTENTS

Section		Page
	PREFACE	1
1	EXECUTIVE SUMMARY	7
	1.1 Purpose and Relevance	7
	1.2 Accomplishments During the Contract Period	8
2	THE MULTIPLE BEAM TELESCOPIC PHOTOMETER EXPERIMENT	12
	2.1 Introduction	12
	2.2 Background and Relevance	12
	2.3 Measurement Requirements	15
	2.4 MTP Optical Design	16
	2.5 Digital Photon-Counting Data System	19
	2.6 Analytical Method	19
	2.7 Experimental Plan	21
	2.8 Experiment Results	24
	2.8.1 Field Operations	24
	2.8.2 Results of the Auroral Structure Experiment; 1 November 1978	24
	2.9 MTP Experiment Conclusions	33
3	GROUND-BASED PHOTOMETRIC SUPPORT FOR DNA/AFGL ROCKET EXPERIMENTS, 1977 – 1978	34
	3.1 Background and Relevance	34
	3.2 Instrumentation and Measurement Capabilities	36
	3.3 Field Widened Interferometer Rocket Experiment	37
	3.3.1 Experimental Plan	37
	3.3.2 Data Summary	39

Section			Page
	3.3.3	Calibrated Scanning Photometer Data	43
	3.3.4	Multibeam Photometer Results: Auroral Motions and E-Fields	44
	3.3.5	FWI Photometric Data Summary	48
3.4	Wideband Multi Support		48
	3.4.1	Experimental Plan	48
	3.4.2	Summary of Auroral Conditions	51
	3.4.3	Calibrated Auroral Intensities and Ionospheric Parameters	51
	3.4.4	Auroral Motions and Electric Fields	54
3.5	SWIR/SWIR/TMA Support		64
	3.5.1	Experimental Plan	64
	3.5.2	SWIR Experiment Data Summary	66
	3.5.3	Calibrated Meridional Photometer Data	66
3.6	Excede II Support		72
4	REFERENCES		74
Appendix			
A	1977 – 1978 DATA SYNOPSIS SHEETS		77

ILLUSTRATIONS

Figure		Page
1	Geometry of the three-beam photometer and MTP experiment	13
2	Schematic diagram of the MTP optical head	17
3	Block diagram of modular photometer, digital data and control systems	20
4	Flow diagram of computer program used to analyze three beam photometer data	22
5	Three color scanning photometer data showing position and mean intensity variations in auroral arcs and forms in magnetic meridian	26
6	Three beam photometer data for period of active auroras, on 1 November 1978 (0950 through 0955UT)	27
7	Total energy deposit versus horizontal distance from zenith for period 0950-0955UT	28
8	Temporal power spectral densities for active aurora interval 0950-0955UT on 1 November 1978	29
9	Horizontal phase velocity (dispersion) plots for active auroral period 0950-0955UT, 1 November 1978	31
10	Spatial PSD plots for period of auroral activity 0950-0955UT, 1 November 1978	32
11	Raw data plot for meridional scanning multispectral photometer	41
12	Three-beam photometer counting rates during period of Field Widened Rocket launch	42
13	Calibrated scanning multispectral photometer data for 427.8 nm and 557.7 nm wavelengths	45
14	Power spectral density of 557.7 nm emission fluctuations observed with the multibeam photometer (3BP1)	46
15	Horizontal phase velocity spectrum for 557.7 nm auroral motions	47
16	Power spectral density of 630.0 nm auroral F-region emission fluctuations measured with multibeam photometer (3B2)	49

Figure		Page
17	Horizontal phase velocity spectrum of 630.0 nm emission fluctuations	50
18	Data plot for 10-min period surrounding WIDEBAND MULTI rocket experiment 28 February 1978	52
19	Three-beam photometer data plot for 0810 to 0815UT period during WIDEBAND MULTI rocket experiment, 28 February 1978	53
20	Total energy deposit versus distance from Chananika for period of the WBM experiment, 20 February 1978	55
21	Average energy of precipitating electron flux plotted versus distance from Chatanika zenith	56
22	Plot of height-integrated Hall conductivities versus horizontal distance from Chatanika zenith during WBM experiment	57
23	Plot of height-integrated Pederson conductivities versus horizontal distance from Chatanika zenith for WBM experiment	58
24	Temporal PSD matrix	60
25	Spatial PSD matrix	61
26	Estimates of auroral electric fields around time of WIDEBAND MULTI rocket experiment; 28 February 1978	63
27	Three-color scanning photometer data for period of SWIR launch on 26 October 1978	67
28	Total energy deposited in the ionosphere versus distance from Chatanika zenith for period of SWIR rocket experiment on 26 October 1978	68
29	Mean energy parameter for precipitating electrons during SWIR launch, 26 October 1978	69
30	Height integrated Hall conductivity for period during SWIR launch, 26 October 1978	70
31	Height-integrated Pederson conductivity for period during SWIR launch, 26 October 1978	71
32	Three-color scanning photometer data for period of EXCEDE launch on 29 October 1978	73

TABLES

Table		Page
1	Rocket launches supported, 1978 –79	9
2	Satellite passes covered	10
3	Measurement requirements	16
4	Three beam photometer and multibeam telescopic photometer specifications	18
5	Photometer operating parameters for 1978 experiments	23
6	DNA/AFGL rocket experiments supported by LMSC ground-based measurements	35
7	Ionospheric irregularities: photometrically measured, and inferred quantities	38
8	FWI experiment: ground optics support plan	40
9	SWIR/SWIR/TMA: ground optics support plan	65

Section 1
EXECUTIVE SUMMARY

1.1 PURPOSE AND RELEVANCE

Ground-based optical spectrophotometric measurements were conducted at the LMSC Chatanika optical research site in support of DNA HAES rocket and satellite experiments during the period 12 September 1977 through 31 December 1978. The purpose of the ground-based photometric measurements was threefold:

- Provide support to the DNA Infrared Field Program rocket launches conducted under the HAES program.
- Provide support for the WIDEBAND Satellite Experiments conducted in coordination with the Chatanika Incoherent Scatter Radar.
- Determine the small-scale structure of auroral emission at 427.8-nm and of OH emission in the 790-nm spectral region by means of coordinated measurements using the MTP (Multibeam Telescopic Photometer) and the three beam photometers at the Chatanika optical research site. These measurements were to provide ground-based support for aircraft measurements of the infrared spatial structure in several bands.

The Chatanika ground-based optical measurements are relevant to the DNA-HAES program goals in the following areas:

- The time and latitudinal history of auroral energy input and its height distribution, and of certain ionospheric parameters, are necessary to an understanding of infrared excitation processes and the temporal and spatial distribution of infrared radiance.
- Multiple beam photometric measurements of auroral and airglow structure are specifically aimed at establishing a data base which may be applied to predictive nuclear effects codes such as ROSCOE.

- Multibeam and scanning photometers provide useful information on auroral and ionospheric parameters which contribute to the generation of ionospheric scintillation effects. These measurements support those made by the DNA/SRI WIDEBAND satellite experiment plus supporting data from the Chatanika incoherent scatter radar. Measurements made in support of WIDEBAND passes are reported elsewhere.

Photometric instrumentation used in the experiments reported herein as well as previous results have been detailed in previous contract reports and publications (References 1–14).

1.2 ACCOMPLISHMENTS DURING THE CONTRACT PERIOD

The Chatanika optical field site was operated for three observing periods during the contract performance period. During these operations, ground-based photometric support was provided to four DNA/AFGL rocket experiments and to 18 WIDEBAND and DMSP satellite passes; successful high spatial resolution auroral and OH airglow structure data were obtained utilizing the MTP; and several coordinated experiments were conducted with the Chatanika incoherent scatter radar. A total of 24 nights of useful photometric data were obtained despite generally poor weather conditions during the fall observing periods. Data synopsis sheets describing each successful night of observations are included as Appendix A.

The ground-based photometric support provided to the DNA/AFGL infrared rocket experiments (plus the WIDEBAND multi) is summarized in Table 1. More detailed descriptions of the experimental plans and results of these measurements are contained in later sections of this report.

The satellite support measurements are listed in Table 2. The detailed results of WIDEBAND support will be reported under separate cover.

The MTP instrument was installed at the Chatanika optical research site and operated in the fall of 1978. Despite unfavorable weather conditions, several nights of successful operation were completed, and high-resolution measurements of auroral structure in the 427.8-nm N_2^+ first negative band, as well as of OH airglow structured emission in the 790-nm spectral region were obtained. The design of the MTP and details of the experimental plan and results are described in this report.

Table 1. Rocket launches supported, 1977–78.

- DNA EXPERIMENTS

Date	Time	Description
11-13-77	0856	Field Widened Interferometer
2-28-78	0811	WIDEBAND Multi
10-26-78	0914	SWIR/TMA
10-29-78	0502	EXCEDE II

- OTHER LAUNCHES

Date	Time	Description
2-27-78	0544	Barium shaped charge (Wescott, University of Alaska)
2-28-78	0417	Barium puffs and TMA trail (Kelley, Cornell University)
3-9-78	0813	Particles and Fields Experiment (Anderson, Rice University)

Table 2. Satellite passes covered.

Date	Time	Satellite
11-11-77	0900	WIDEBAND
	1030	WIDEBAND
11-12-77	0940	WIDEBAND
11-13-77	1010	WIDEBAND
2-28-78	0952	WIDEBAND
3-1-78	0846	WIDEBAND
	1031	WIDEBAND
3-2-78	0926	WIDEBAND
3-4-78	0820	WIDEBAND
10-26-78	1037 UT	DMSP
10-29-78	0831	WIDEBAND
10-31-78	0950	WIDEBAND
	1031	DMSP
11-1-78	1014	DMSP
	1030	WIDEBAND
11-2-78	0925	WIDEBAND
	0956	DMSP
	1110	WIDEBAND

Finally, coordinated experiments conducted in collaboration with the SRI International incoherent scatter radar group provided further successful cross calibrations between measurements made utilizing the radar technique and the optical technique. These cross-calibration efforts are valuable because not only do they increase the confidence that each technique is providing accurate information, but they allow the instruments to be used to support rocket and satellite experiments in a complementary manner with confidence that equivalent ionospheric and auroral properties are measured with comparable accuracy and precision. The results of coordinated experiments conducted at Chatanika will be reported in the open literature.

Section 2
THE MULTIPLE BEAM TELESCOPIC PHOTOMETER EXPERIMENT

2.1 INTRODUCTION

In this section the background, relevance, and requirements for high spatial resolution measurements of OH airglow structure and of auroral structure in the 427.8-nm first negative band emission of N_2^+ are presented. The optical design of an instrument (MTP) intended to measure such structure is described. Typical results on auroral spatial structure obtained during the fall 1978 observing period are summarized.

The MTP instrument is an extension of the three-beam photometers (3B) developed and fielded for DNA which have been used to determine the spatial structure and statistical properties of emission in various auroral and airglow spectral regions. The 3B instruments cover horizontal scale sizes in the 10's of km range. When it became apparent that currently used and prospective defense systems required a data base in certain spectral regions extending to a few hundred meters scale size, the MTP was designed and fielded to accommodate these requirements. Figure 1 illustrates the concept of the multibeam photometer experiment.

2.2 BACKGROUND AND RELEVANCE

The upper atmosphere below about 120 km or so exhibits neutral density fluctuations which are the result of turbulent effects or which are caused by upward propagating wavelike disturbances. The mean amplitude of these turbulentlike and wavelike disturbances varies from less than 1% to values exceeding 10% of the mean density. When this natural field of irregularities is subject to nuclear burst ionization and excitation, the irregularity field may provide an equivalent irregularity structure in both ionization and in nuclear induced IR emission. To the extend that

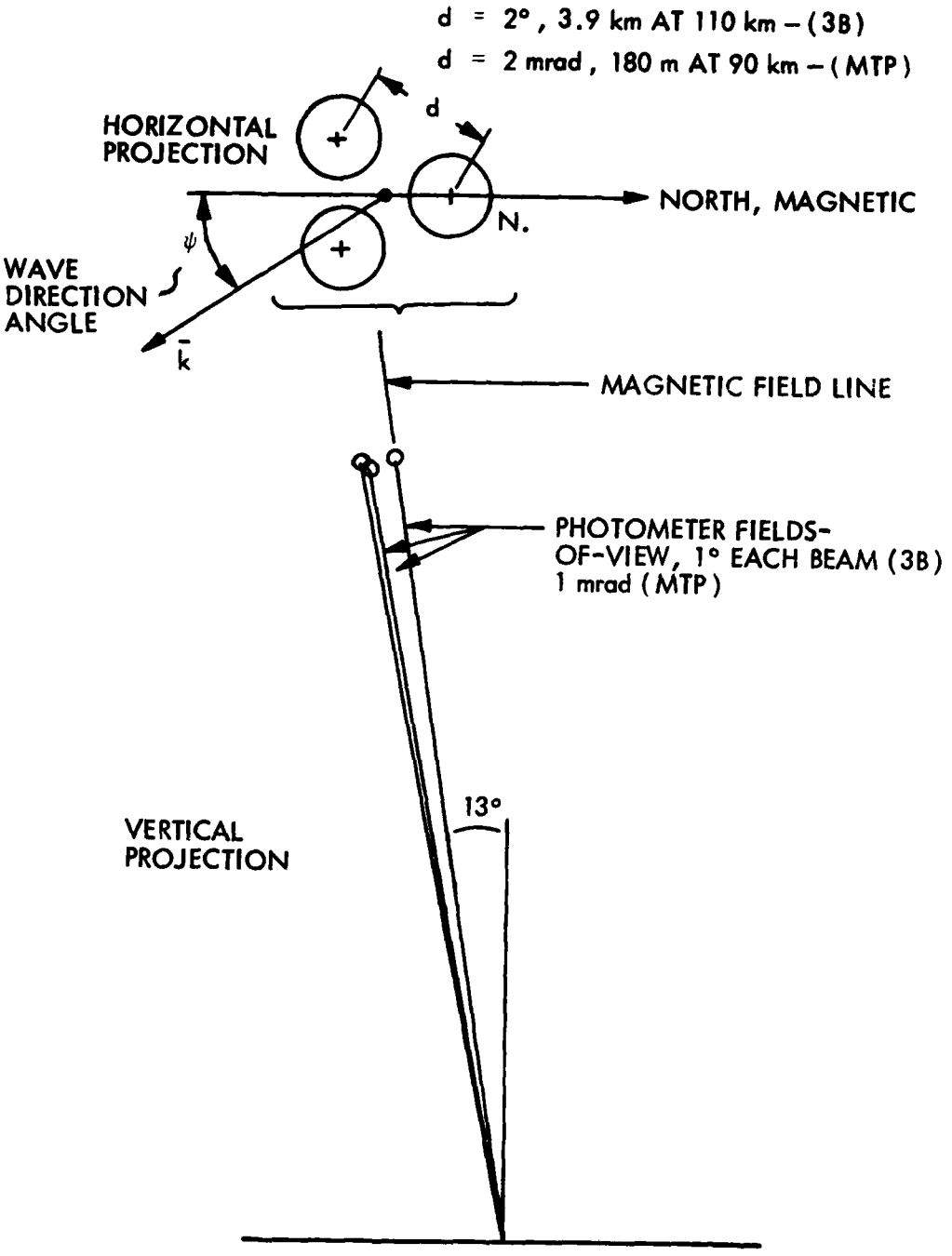

Figure 1 Geometry of the three-beam photometer and MTP experiment.

the excited state population and equivalent IR radiance structure may lead to degradation of IR systems, then the natural atmospheric irregularity field must be characterized statistically to determine the nuclear IR systems effects.

High-altitude nuclear bursts typically deposit the major fraction of their energy as x rays in the 60- to 120-km-altitude range. In this range, the vertical structure of the atmosphere changes greatly in that in the lower region (the upper mesosphere) turbulent and wavelike neutral density fluctuations typically are growing, whereas in the upper region above the mesopause the temperature gradient is positive and neutral disturbances are either ducted or are damped out by kinematic viscosity.

The scale sizes of turbulent and wavelike irregularities in the region of interest vary from some inner scale, below 100 m or so, to an outer scale which may be larger than the local scale height, i.e., greater than 6 km or so. Typical temporal scales for neutral disturbances range from tens of seconds to over 1 hr. The forms of the disturbances in their classical descriptions range from Kolmogorov inertial turbulence and buoyant turbulent effects through acoustic waves to ducted acoustic gravity waves having wavelengths of hundreds of kilometers.

Measurements have been made (References 15–16) of OH airglow structure in both the photographic infrared and in the SWIR spectral regions. This structure exhibited obvious scale sizes in the range of tens of km but no attempts had been made to analyze the data in terms of spatial PSDs, which are the statistical parameters required in the nuclear IR effects prediction codes. Spatial PSDs of OH and other species' emissions have been measured under DNA sponsorship using the 3B photometers. Extension of these measurements to the 100-m scale sizes is now possible using the MTP instrument.

Because the excitation processes are reasonably well known for the OH Meinel bands (which extend from the 500-nm region to wavelengths greater than 4 μm), measurements of spatial PSDs made in the near IR ($\lambda \sim 790$ nm) can be used to model the SPSDs in IR bands of importance to defense systems.

Measurement of auroral emission structure in the N_2^+ first negative band presents a similar problem to that of OH structure. Because the 427.8-nm emission results from an allowed transition, i.e., its radiative lifetime is very short, the

427.8-nm structure accurately reflects the structure and motions of the precipitating particle flux. Auroral electron precipitation is highly structured in space and time, reflecting the effects of as yet undetermined plasma instability processes. Likewise, the beta aurora resulting from a high-altitude nuclear burst is highly structured, although it is also indeterminate at present whether the plasma instability processes responsible are physically identical, or even similar to those in natural auroras.

Even though further detailed experimental and theoretical studies of auroral precipitation processes may lead to a better understanding of the nuclear beta aurora, a more immediate application exists for auroral structure data, e.g., characterization of prompt versus delayed IR excitation and emission processes, and spatial and temporal PSD determination for both input energy and output IR radiance structure. For example, by utilizing an analytical technique developed by Kumer (17), one is able to relate the spatial structure of CO_2 emission in several bands to the spatial and temporal behavior of the input auroral energy. Hence, measurement of spatial and temporal PSDs for auroras will assist in modeling both natural auroral and nuclear burst beta auroral effects in IR spectral regions which can significantly degrade defense systems performance.

2.3 MEASUREMENT REQUIREMENTS

As described in the introductory section, very high spatial resolution measurements of OH airglow emission in the 0.8-μm spectral region, and auroral emission measurements in the 0.4- to 0.6-μm region are required. From such measurements the statistical power spectral densities in spatial and temporal coordinates are derived, such that they may be applied to IR radiance fluctuation models. The range of emission intensity and spatial and temporal resolutions are wide; therefore, the optical head as well as the electronics subsystems must be carefully designed to respond to the data requirements. The measurement requirements for the MTP are quantitatively summarized in Table 3 for the range of conditions expected to be experienced in the field.

Table 3. Measurement requirements.

Parameter	Airglow Case	Auroral Case
Wavelength	770.0 – 810.0 nm	427.8 nm
Emitting Species	OH	N_2^+
Intensity Range Expected	0.5 to 2 krad	100 R to 100 krad
Spatial Structure		< 0.1 to > 100 km
Turbulentlike	0.1 to 10 km	
Wavelike	10 to 100 km	
Temporal Variations	10's of s	0.1 to 10's s

2.4 MTP OPTICAL DESIGN

The MTP instrument operates essentially as three independent photometers having certain common components: the objective lens, collimation lens, and filter. This instrument is illustrated in Figure 2. The field-of-view of the instrument is defined by the three-hole field stop behind which the collimator and condenser lenses focus the images of the individual field stop regions on the photomultiplier detectors.

The sensitivity of the MTP is defined by the following equation:

$$S\ (\text{cts/Rayleigh-s}) = T\ A\ Q\Omega\ (10^6/4\pi)$$

where

- I = intensity in Rayleighs
- T = overall instrument transmission
- A = objective collecting area
- Ω = solid field-of-view in each beam
- Q = quantum efficiency of the detector

The optical transmission and quantum efficiency of a photometric system such as the MTP can be optimized to a certain extent, but the fundamental limitations on

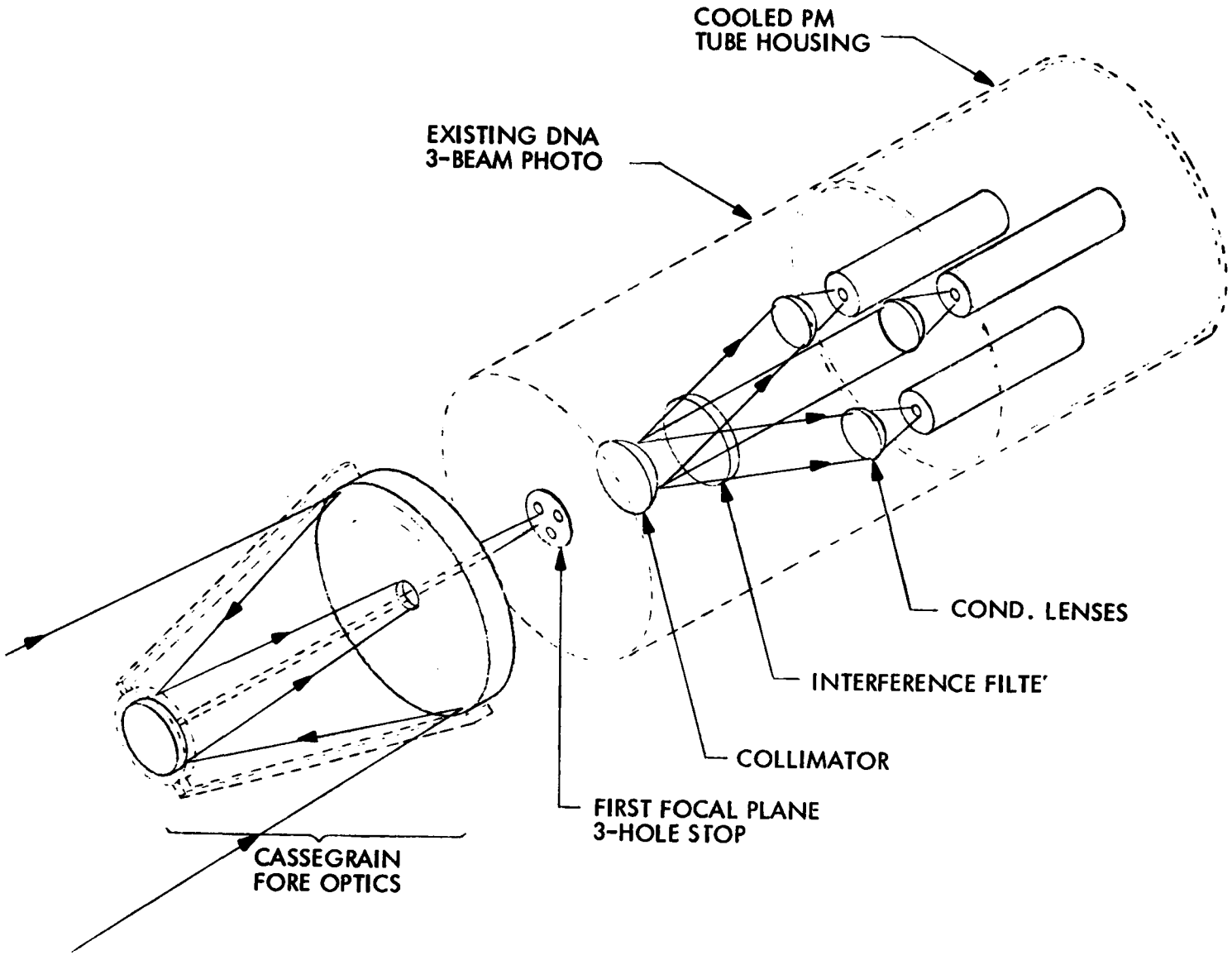

Figure 2. Schematic diagram of the MTP optical head.

the system sensitivity will be the value of the $A\Omega$ product. In this case, limited choice in values of the total collection area exists because of the existing collector optics. For the MTP, the 18-in.-diameter cassegrain telescope owned by DNA and formerly used on the TIFIS system was selected. However, the quantum efficiency of the detector in the 0.8-μm region was improved by use of high gain extended red photomultiplier tubes which were not available when the original multibeam photometer was designed and built. Finally, careful selection of filters, especially in the 0.8-μm spectral region to optimize their transmission also represents an improvement in sensitivity over the original 3B design. The design parameters for the MTP compared with those of the 3B are summarized in Table 4.

Table 4. Three beam photometer and multibeam telescopic photometer specifications.

Parameter	3B	MTP
Objective Area	40 cm^2	1460 cm^2
Focal Length	18 cm	267 cm
Filter Wavelengths	427.8 nm	427.8 nm
	557.7 nm	630.0 nm
	630.0 nm	770.0 nm
PM Tube Quantum Efficiency		
427.8 nm	20%	20%
770.0 nm	0.3%	2%
Field-of-View (mrad)	16	1
Beam Separation	2 × FOV	2 × FOV
An Ω Product	9.6×10^{-3}	1.2×10^{-3}
Sensitivity		
427.8 nm	50 cts/R-s	5.7 cts/R-s
770.0 nm	0.7 cts/R-s	0.6 cts/R-s

Table 4 shows that the high-resolution measurements of OH emission in the 0.8-μm spectral region can be made with a sensitivity equivalent to the original 3B instrument, e.g., about 0.6 cts/R-s, for a 1-mrad FOV. If better counting statistics are required for very low values of OH emission intensity, then the FOV can be modified to 3 mrad by substitution of the focal plane field stop and the collimating lens.

2.5 DIGITAL PHOTON-COUNTING DATA SYSTEM

A digital data system was developed under past DNA-sponsored ionospheric irregularities programs which incorporates photon-counting capabilities, computer interface features, modularity such that expansion to as many as 50 photometer channels can be accommodated, and digital control interfaces. This system is outlined in block diagram in Figure 3.

Prior to the DNA-sponsored work which began in 1970, efforts made to measure the temporal power spectral densities of airglow emission features indicated the requirement for digital photon counting rather than analog recording of the data because of the very wide dynamical range which can be accommodated and the ability to compute PSDs all the way in power down to the photon noise limit without regard for system noise. In the present digital data system, the limiting noise factor is the dark emission from the photomultipliers, much of which is eliminated by cooling the detector tubes. The data system configuration which was used to support the MTP instrument measurement program in Alaska was the present 10-channel system.

2.6 ANALYTICAL METHOD

Analytical routines were devised during the early stages of the Ionospheric Irregularities program to facilitate computation of both temporal power spectra and spatial power spectra from the multispectral photometer (MSP) and the three-beam photometer (3B). The available software for reduction and analysis of the photometer data consists of a series of individual programs which are summarized below:

- COPY: Copies the digital tape from the field onto a library tape and verifies the contents

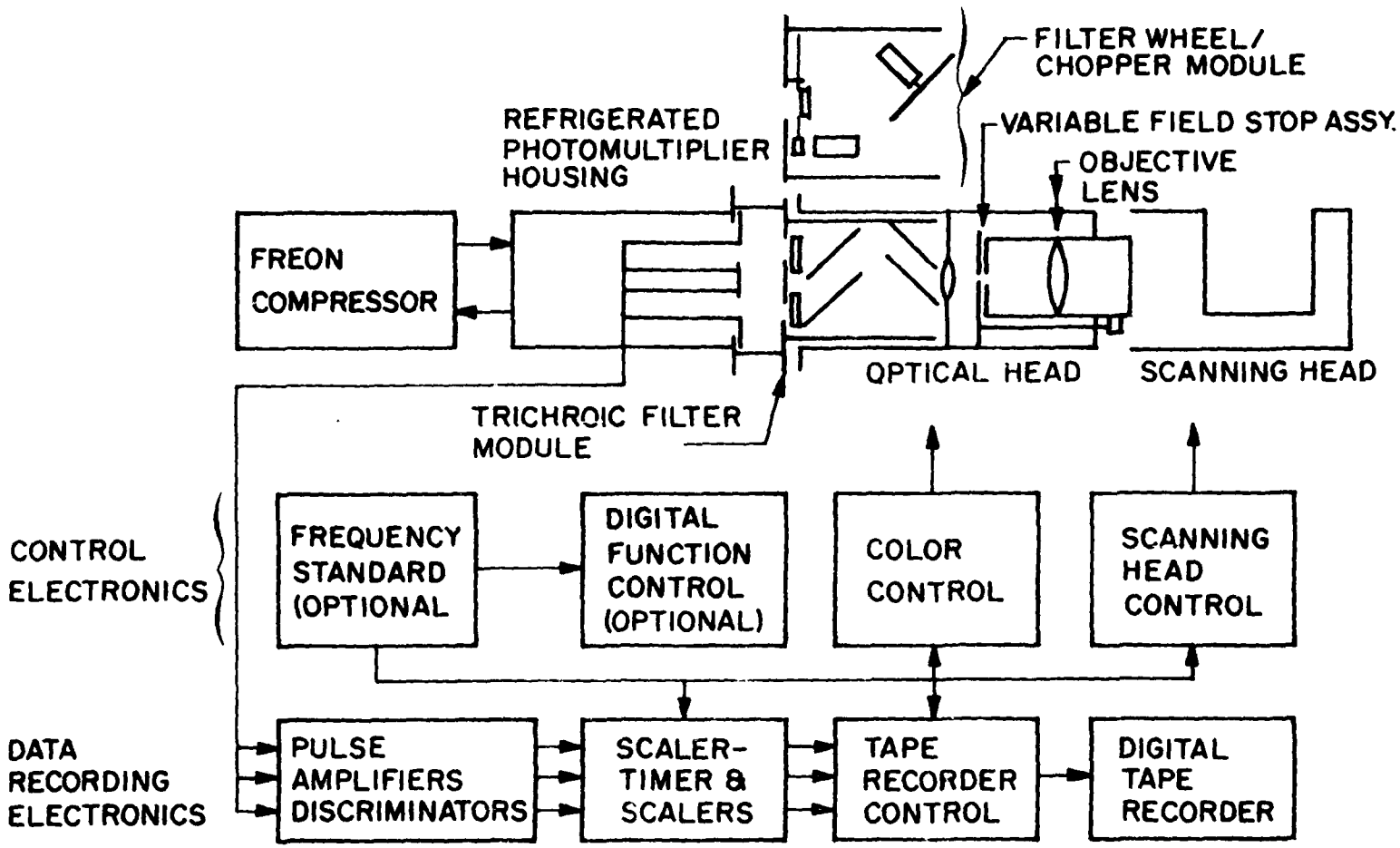

Figure 3. Block diagram of modular photometer, digital data and control systems.

- EDIT: Provides a frame-by-frame pictorial output of the raw data
- NUCAL: Provides calibrated output of desired channels plus intensity ratios in several formats
- NUWAV: Provides statistical analyses of single and multibeam photometer data
- CONX: *

The principal results of this program, PSDs, horizontal velocity dispersion, and associated statistical data were obtained from the NUWAV code.

The operational features of the code are best described by reference to Figure 4. Here, the code's operational features showing how the 3B and MTP input data are processed to yield spatial and temporal PSDs plus all of the necessary diagnostic information are summarized schematically.

2.7 EXPERIMENTAL PLAN

The multiple beam telescopic photometer (MTP) was fielded at the LMSC Chatanika optical research site in the fall of 1978. In addition to the MTP, other photometric instrumentation at the research site includes a three-beam photometer (3B) and a multispectral scanning photometer (MSP). These DNA-owned photometers are controlled by, and have data interfaces to, a DNA digital data and control system the functions of which were described in section 2.4. These instruments were operated in several modes depending upon the degree of auroral disturbance.

The following specific measurements were conducted:

(1) Quiet Period OH Emission Structure. The MTP and 3B instruments were operated to determine spatial and temporal structure in the OH airglow emission. The MSP instrument was utilized to ensure that auroral contamination to the OH airglow radiance was minimized.

(2) Disturbed Period OH Emission Structure. Because the relatively wide filter passbands in the MTP and 3B units allow contamination of OH airglow

*An upgraded version of NUCAL provides calibrated photometric intensities, energy input, energy parameter, and ionospheric Hall and Pederson conductivities in a variety of formats.

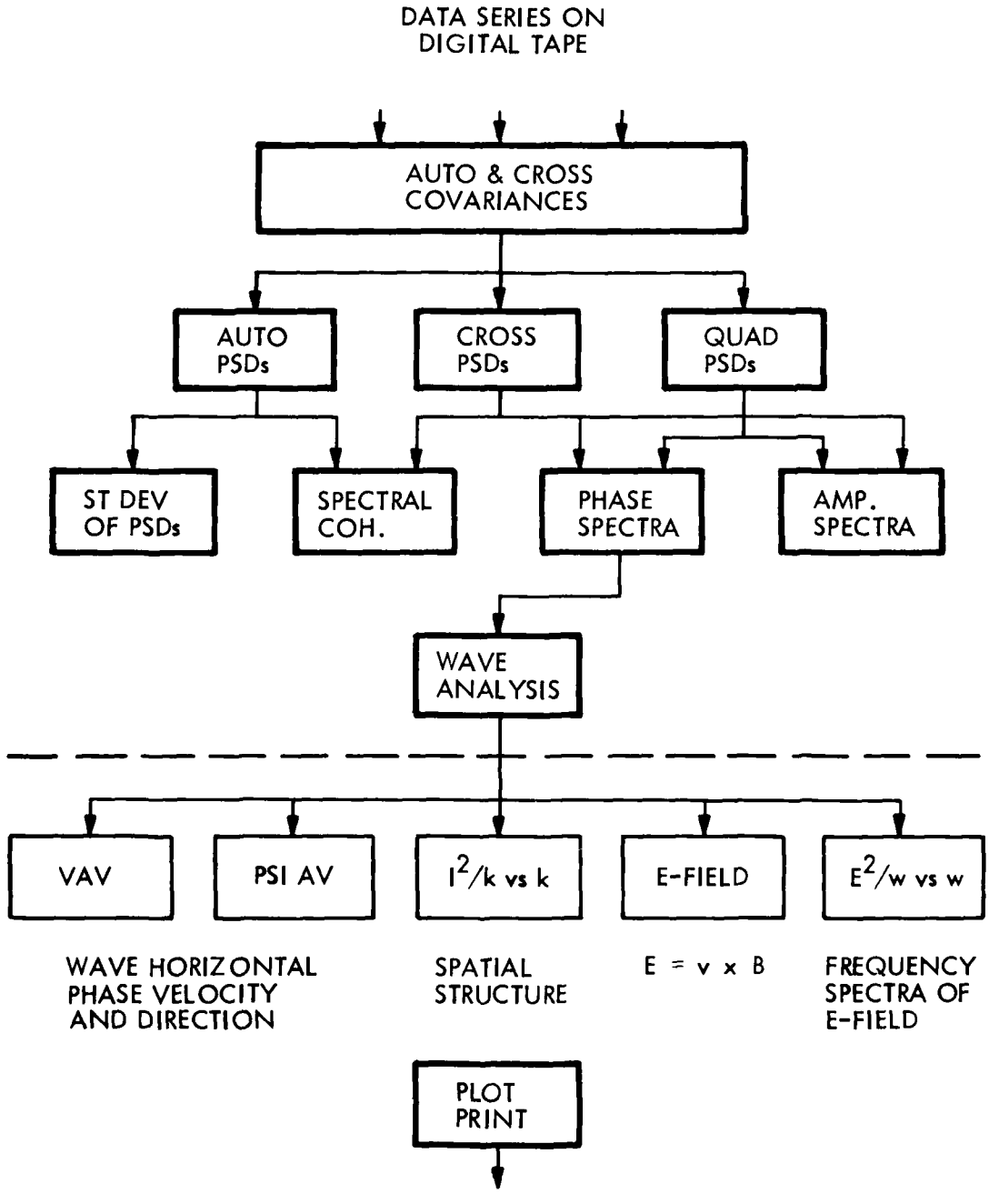

Figure 4 Flow diagram of computer program used to analyze three beam photometer data. The improved subroutines for obtaining average phase velocity, direction, etc. are those indicated below the dashed line.

intensity by near IR auroral emissions, it is impossible to interpret the OH data uniquely in the presence of auroras without independent measurement of the auroral intensity fluctuations. This will be provided by the MSP, operated in a zenith orientation coinciding with the MTP and 3B units. By this method we hope to determine OH structure during mildly disturbed periods.

(3) Auroral Emission Structure. Short time-scale measurements of auroral emission fluctuations were obtained by operating the MSP and 3B instruments on a short-time base and filtering for one of the prompt auroral spectral emissions such as 427.8 nm. This improved temporal resolution may be attained because auroral emission is much more intense than background OH airglow emission, at least in the visible-near IR spectral range.

A summary of the experimental configurations and instrument parameters planned for the above experiments is contained in Table 5.

Table 5. Photometer operating parameters for 1978 experiments.

Parameter	MTP	3B	MSP
Wavelength	770.0–810.0 nm (1, 2) 427.8 or 557.7 nm (3)	770.0–810.0 nm (1, 2) 427.8 or 557.7 nm (3)	427.8, 557.7 nm 630.0 (or 770.0 nm)
Field-of-View (each beam)	1 mrad	17 mrad	50 mrad
Angular Resolution	2 to 6 mrad	34 mrad	50 mrad
Temporal Resolution	1 s (1, 2) ≤ 0.5 s (3)	1 s (1, 2) ≤ 0.5 s (3)	1 s (1, 2) ≤ 0.5 s (3)
Integration Time	300 s (1, 2) 30 s (3)	300 s (1, 2) 30 s (3)	
Orientation	Zenith (1, 2, 3)	Zenith (1, 2, 3)	Zenith (2) Scanning (1, 3)

Note: Numbers in parentheses indicate the number of the experiment as described in the text. Explanation of the meaning of the individual parameters and their relationship to experimental goals is contained in Section 2. MTP specifications are believed to be those attainable with the system but are subject to modification as MTP design is finalized. Attainable spatial and temporal resolutions also depend upon the intensity of the spectral emission observed.

2.8 EXPERIMENT RESULTS

2.8.1 Field Operations

The MTP was shipped to the field and installed in a fixed mount within the LMSC optics van at Chatanika. We chose to use the MTP in a fixed mount, oriented toward magnetic zenith rather than having a fully steerable mount for two reasons: reduction of cost by simplification of the mechanical construction required; and maximization of usable data by pointing constantly at geomagnetic zenith. Because of the very narrow FOV of the MTP, auroral structure data taken away from geomagnetic zenith would be difficult to interpret because of the inclination of the instrument line-of-sight with respect to the magnetic field line direction. Hence, both scientific and cost considerations supported use of a fixed mount.

The MTP was installed and tested during the period 23 to 29 October. All subsystems were thoroughly checked out and operation of the system was verified during a number of dark-current runs. After filters were installed and final calibrations carried out, we were able to conduct a number of data runs despite the generally very poor weather conditions.

In addition to the MTP instrument, the existing three color (3C) and three beam (3B) instruments were operated in conjunction with the digital photon counting data system.

In the following section, the results of operating the combined MTP, 3B, and 3C photometers during a period of intense auroral activity are described. Although quiet-time OH airglow data were obtained also during this operation, an optimum data set has not been picked as yet, principally because of interference by poor weather conditions.

2.8.2 Results of the Auroral Structure Experiment; 1 November 1978

Auroral Conditions. Auroral activity was noticeable as soon as the sky became dark enough to discern the intense, active forms. The activity continued throughout the

period of observations. The data segment described in this report (record 67, 0950-0955U) covers a period when three distinct arcs were visible, with the instrument FOVs just to the poleward edge of the middle arc. Prior to this time, the arc systems were very intense and active as is illustrated in the scanning photometer records presented in Figure 5. Just before the data segment began, the two southward arcs diminished greatly in intensity and in mean energy. The northward arc remained essentially stationary and at the same intensity. During the data segment analyzed herein, the two southward arcs intensified approximately a factor of 10 in total energy and the mean energy parameter also increased significantly, thus lowering the mean altitude of ionization and emission. Because the instrumental FOVs were located just off the edge of the middle arc, the total photometric intensity observed during this data interval did not change commensurate with the total arc intensity as illustrated by the raw data from the MTP and 3B1 instruments in Figure 6. However, both instruments observed a high degree of structuring and concurrent rapid horizontal motions as may be discerned by displacements of the intensity peaks from channel to channel in the two instruments.

Plots of calibrated total energy deposit versus distance from Chatanika are illustrated in Figure 7. The positions of the MTP and 3B1 instrument fields-of-view are indicated in this figure.

Structure Analysis. The NUWAV code was applied to the MTP and 3B1 data as discussed in previous sections. Examination of the statistical parameters describing the signal-to-noise ratio and data quality indicate that excellent results were obtained on this particular data segment as well as on the entire data interval examined to date. Three questions were addressed in our preliminary analysis: (1) how do the temporal PSDs of the auroral intensity fluctuations change with the spatial scale of the measurement, e.g., MTP resolution versus 3B1 resolution; (2) do the velocity spectra of the auroral fluctuations vary substantially with spatial scale; and (3) what are the spatial PSDs as measured by the two instruments.

Temporal PSDs from the two instruments are illustrated in Figure 8. Here it is apparent that the two instruments observe essentially identical low-frequency intensity

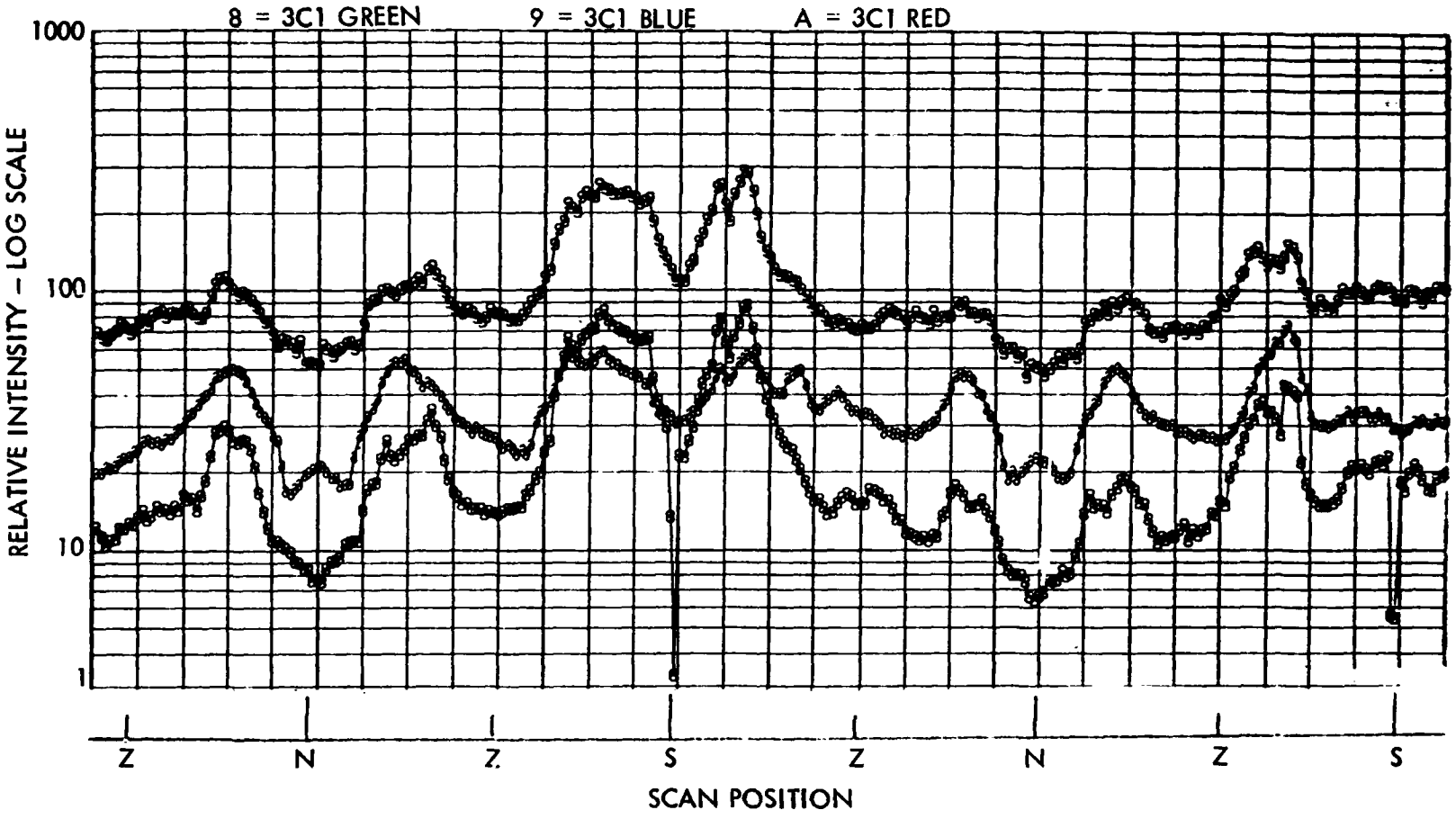

Figure 5. Three color scanning photometer data showing position and mean intensity variations in auroral arcs and forms in magnetic meridian. Note that the position of the three beam photometers' FOV is just poleward of a strong emission feature during this time segment, with the strongest and most energetic display farther to the south. Data were obtained during same interval on 1 November as those illustrated in Figure 6.

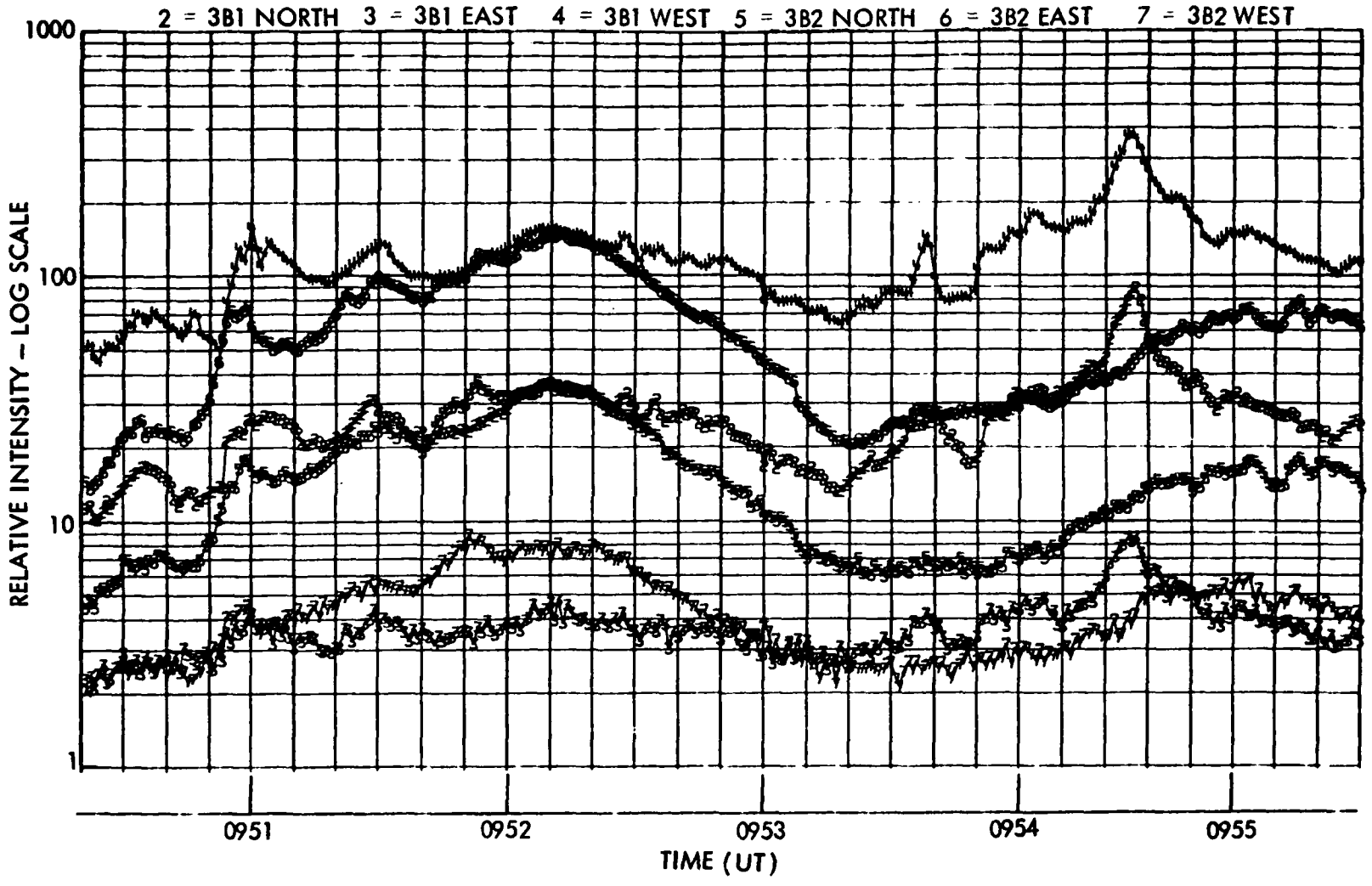

Figure 6. Three beam photometer data for period of active auroras on 1 November 1978 (0950 through 0955UT). Both photometers operating on 427.8 nm wavelength. Channels 2 through 4 represent 3B1 data; channels 5 through 7 represent MTP data. Mean intensities and dynamical ranges appear somewhat different because of differences in counting efficiency and dark count levels.

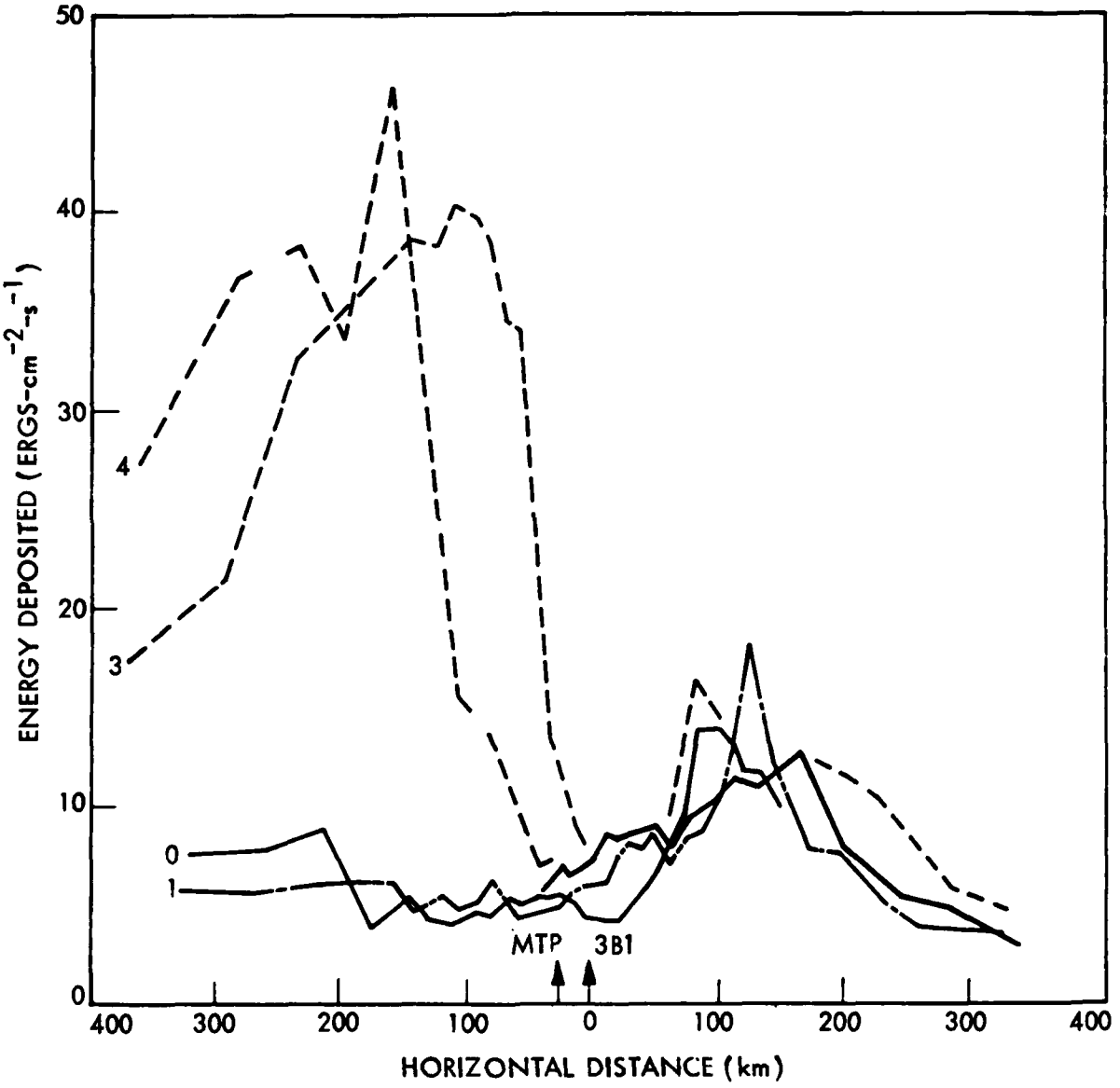

Figure 7. Total energy deposit versus horizontal distance from zenith for period 0950-0955UT. Three scans (0,1,2) before breakup are depicted by solid lines. Two scans (3,4) after breakup are depicted by broken lines.

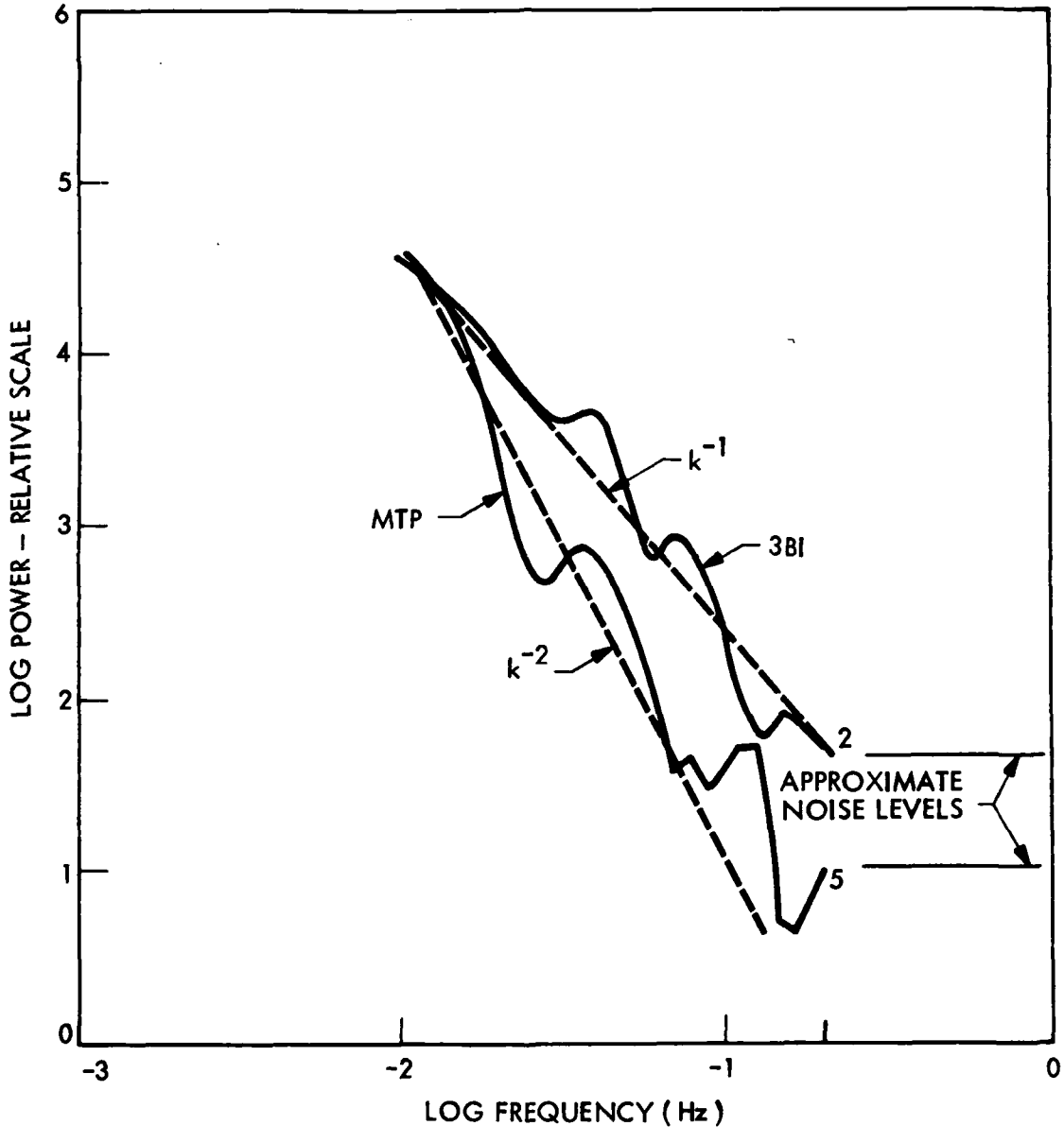

Figure 8. Temporal power spectral densities for active aurora interval 0950-0955UT on 1 November 1978. Note that each spectral estimate curve closely follows a power spectrum law of the form $P = P_o k^{-n}$.

fluctuation content but the frequency response, the fall-off at higher frequencies differs somewhat. The accuracy of computation of temporal PSDs under the present NUWAV scheme is approximately 30%, hence the differences at higher frequencies are significant statistically. It is indeterminable at present whether the difference in average slope (k^{-2} for MTP, k^{-1} for 3B1) between the two instruments represents the effects of somewhat different FOV (the MTP was closer to the arc) or their differing spatial resolutions. It is encouraging to note, however, that the subsidiary peaks in the 0.03- to 0.1-Hz spectral range reproduce, thus indicating that both instrument responded similarly to coherent fluctuations in auroral intensity.

The velocity spectra for the two instrumental data sets are highly structured, but after manually smoothing the data, one may deduce that the average velocity did not change appreciably over the frequency range of interest, 0.01 to 0.2 Hz. The cuspid behavior of the velocity spectrum from the wider FOV instrument, 3B1, indicates that significant auroral structure existed on a scale comparable with the horizontal resolution of the instrument, about 8 km (Figure 9). Interpretation of the velocity minimum values in terms of the auroral electric fields in the arc's vicinity indicates that the electric field structuring as well as its absolute magnitude are significantly reduced on a small scale, as evidenced by the lower velocities exhibited on the MTP instrument. The velocity irregularities exhibited by the MTP instrument as well as some of those shown in the 3B data are mainly the result of statistical error in the estimation of the temporal PSDs. Velocity data depicted here should be considered to have an accuracy of about 30 to 50%. A statistical smoothing procedure will be instituted during more detailed analysis of these data in order to improve PSD and associated quantities derived therefrom.

The temporal PSD and velocity spectra were used to compute the spatial PSDs for the data sets from the MTP and 3B1 instruments. Figure 10 depicts these results for the data interval discussed in this report. Most notable is the relatively slowly increasing SPSD over the range of 0.1 to about 1 km^{-1} spatial frequency, and the rapid decrease in SPSD value at higher spatial frequencies. The data set reported herein appeared to contain significant spatial intensity fluctuations to spatial frequencies as high as about 6 km^{-1}, which corresponds to a spatial wavelength of about 1 km

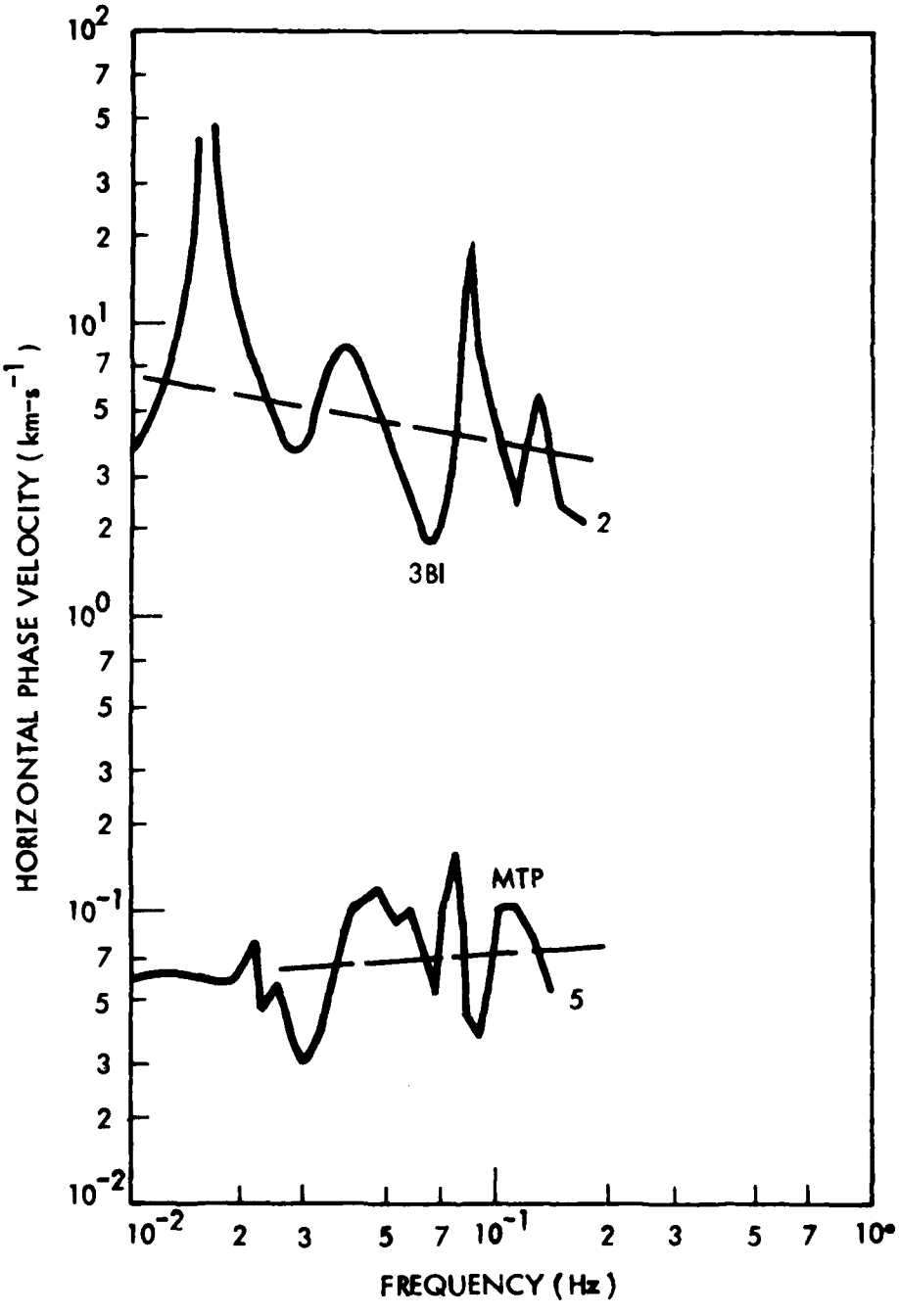

Figure 9. Horizontal phase velocity (dispersion) plots for active auroral period 0950-0955UT, 1 November 1978.

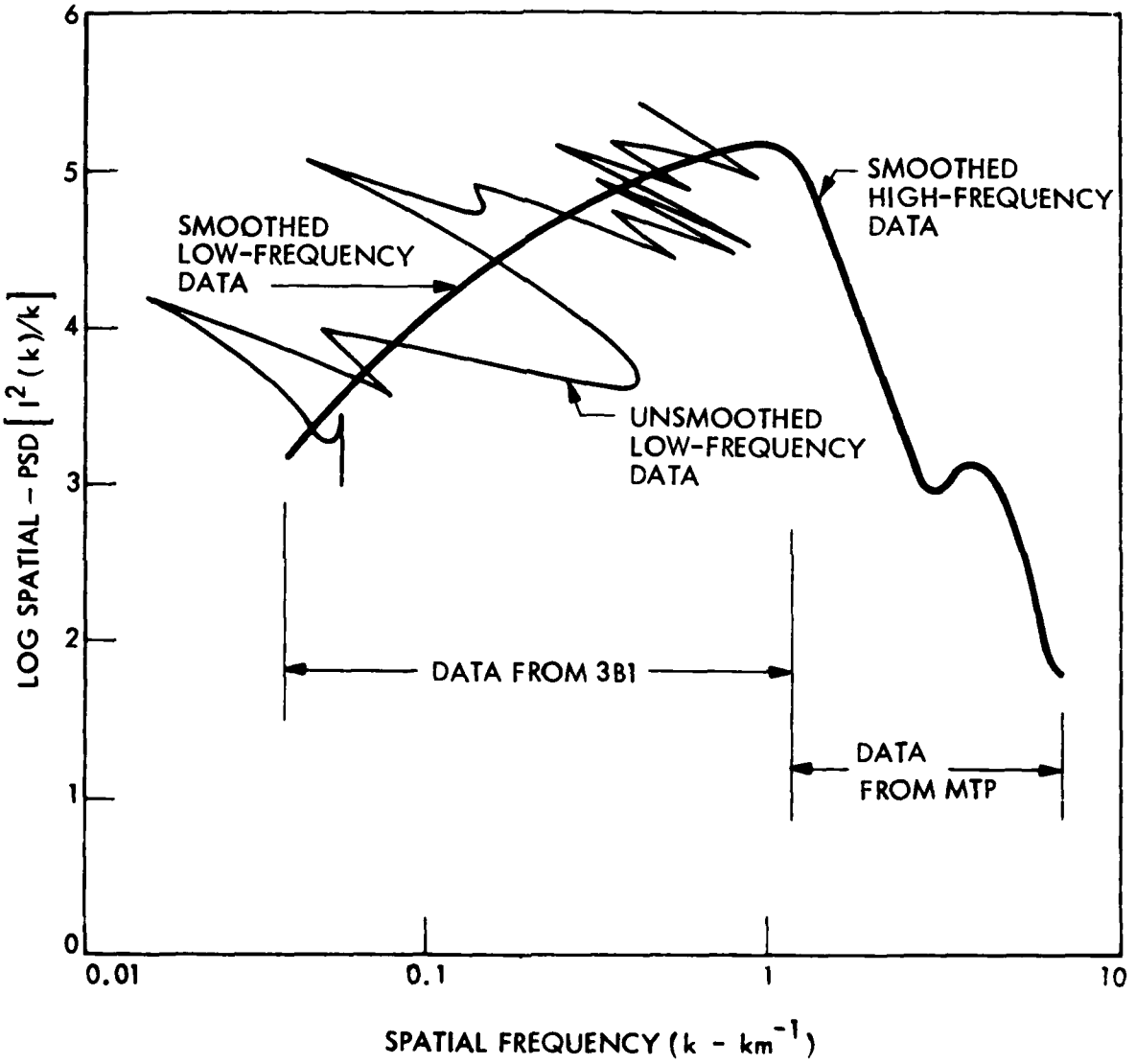

Figure 10. Spatial PSD plots for period of auroral activity 0950-0955UT, 1 November 1978. Note degree of smoothing required at low frequencies to fit data to high frequency portion of curve derived from MTP. Turnover of SPSD at spatial frequency of about 1 km^{-1} (wavelength of 6 km) appears to be typical of results to date.

(full quasi-sinusoidal wavelength). The differences between the manually smoothed data and the inherently noisy computer results are apparent. It is clear that more effective SPSD smoothing routines must be incorporated in the NUWAV code in order to provide fully usable SPSD data to the modeling community.

The results presented herein depicting TPSD, velocity spectra, and SPSDs are typical for the data interval 0950 to 1030UT which was analyzed in detail. We have not presented the entirety of the data because of the necessity for improving the smoothing routines as well as making the computer plot outputs more compatible with the input requirements of the modeling community. These tasks will be undertaken during the follow-on analysis of the entire data library.

2.9 MTP EXPERIMENT CONCLUSIONS

The results of the combined MTP and 3B photometer experiments aimed at defining the spatial fluctuation characteristics in active auroras, to date, indicate that combined use of the two three-beam instruments having differing spatial resolutions is a powerful technique for obtaining the SPSD data required by the nuclear effects modeling community over a range of spatial frequencies about 0.01 to 10 km^{-1}. Although the data presented herein were mainly indicative of the results which can be obtained, and also showed some of the computational and analytical problems still present in our NUWAV code, the results as a whole are very promising. We anticipate that after some relatively minor improvements to the NUWAV code, analysis of the auroral and OH data base will enable the generation of a family of high quality SPSD data which can be used to generate and evaluate predictive codes for high-altitude burst generation of structured spatial radiance in various wavelength regions of interest.

Section 3

GROUND-BASED PHOTOMETRIC SUPPORT FOR DNA/AFGL ROCKET EXPERIMENTS, 1977 – 1978

3.1 BACKGROUND AND RELEVANCE

LMSC has provided ground-based photometric support to the DNA HAES program at Chatanika and Poker Flat, Alaska, since the inception of the ICECAP program in 1972. Specific HAES program elements supported include ICECAP, EXCEDE, COMMOCAP, and WIDEBAND. A total of over 400 hr of useful photometric data have been obtained from 1972 to date in support of 20 DNA/AFGL rocket launches and numerous DMSP and WIDEBAND satellite passes (1977 – 1978 only). These operations are listed in Table 6. With the exception of two launches in 1974, the digital photometer system has a record of perfect operation and data recovery. Additional periods have also been scheduled for coordinated photometer SRI incoherent scatter radar experiments to establish the cross-calibrations previously discussed.

The relevance of our ground-based photometric measurements to the infrared rocket experiments may be summarized as follows:

- A time history of the energy deposited in the vicinity of the rocketborne sensor by various auroral processes is essential to unfolding the excitation history of several IR bands which are important to systems.
- Ground-based measurements of the spatial structure of emitting species and in the IR excitation sources assist in separation of spatial and temporal effects as the rocket traverses the emitting region.
- Ground-based measurements of the intensities of several bands of interest assist in calibration of rocketborne instrumentation.
- Ground-based observations assist in placing the rocket data in the proper context of auroral morphology and phenomenology.

Table 6. DNA/AFGL rocket experiments supported by LMSC ground-based measurements.

Date	Launch UT	Rocket Experiment
3-6-72	1214	OH Photometer
3-9-72	1052	CVF IR Radiometer
3-21-73	1011	OH Photometer (Quiet condition)
3-22-73	1213	CVF, LWIR Radiometer
3-24-73	1031	Multipayload, SWIR
3-27-73	0938	CVF, SWIR Radiometer
2-21-74	0916	HIRIS, LWIR Interferometer
2-25-74	0738	CVF, SWIR Radiometer
3-4-75	0740	OH Radiometer
3-10-75	0912	LWIR Radiometer
3-11-75	0633	E-field Rocket
3-12-75	0748	Multipayload
4-13-75	0946	EXCEDE
2-28-76	0547	EXCEDE
11-19-76	0406	EXCEDE
11-26-76	1025	WIDEBAND
11-13-77	0855	Field Widened Interferometer
2-28-78	0811	WIDEBAND-Multi
10-26-78	0914	SWIR/TMA
10-29-78	0502	EXCEDE II

The measurements reported herein utilize DNA-owned photon-counting digital photometers presently located at the LMSC optical research site at Chatanika. Unlike many of the existing instruments such as range support instrumentation, photometers, spectrometers, etc., the DNA apparatus was specifically designed to address the problems of importance to the HAES program; namely the physical processes taking place in the quiet and disturbed upper atmosphere which are related to the processes induced by upper atmospheric nuclear bursts. To this end, not only the instrumentation directly supports HAES program requirements, but the data reduction and analysis software is designed to provide the results most relevant to the HAES program elements. Brief summaries of the instrumentation and measurement capabilities are contained in the following section.

3.2 INSTRUMENTATION AND MEASUREMENT CAPABILITIES

The photometric instrumentation consisting of the multichannel digital photon-counting photometer system is currently installed and operational at Chatanika, Alaska. This system incorporates several types of optical heads, coupled to a common ten-channel digital photon counting and data recording system. The overall photometer system configuration was illustrated in Figure 3. The photometers serve several purposes with respect to HAES measurement goals. These are summarized as follows by instrument type:

- Trichroic (Three Color) Photometer (1). This instrument is designed to monitor auroral emissions in three spectral regions such that the energy deposit characteristics can be defined. It is usually operated in a meridional scanning mode. One unit is currently installed at Chatanika.
- Multibeam (Three Beam) Photometers (2). These instruments are designed to monitor the horizontal drift of emission irregularities in either the quiet or auroral disturbed ionosphere. When quiet, the horizontal wind velocity and spatial structure (PSD) in the emitting region can be inferred. During auroral disturbances, the horizontal motion of auroral emission is used to infer the electric fields. Auroral emission PSDs are also obtained.

- Telescopic Three-Beam Photometer (1). This instrument is designed to monitor the same quantities as the previously described three-beam unit, except upon a much finer horizontal resolution scale, 200 m versus 2 km. This unit was installed at Chatanika during the Fall of 1978.

Operational parameters describing these photometers were summarized in Table 4. The details of their optical and electronic design are contained in References 1 and 2 and in section 2.3 of this report.

The photometric instrumentation described may be used to monitor a wide variety of upper atmospheric spectral emission characteristics for both quiet times and for aurorally disturbed conditions. The capability for interpretation of the basic photometric measurements (i.e., calibrated spectral intensities versus space and time) in terms of quantities important to the HAES program experiments has been developed over a long period of DNA support, since first operations began in 1972. The details of data reduction, interpretation, and analysis are contained in previous DNA reports listed as References 3 through 11 and in open literature publications, References 12 through 14. It should be noted that much of the open literature work has been the direct result of DNA support, and has resulted from close collaboration with the SRI Incoherent Scatter Radar group.

The most effective method to summarize the measurement capabilities of the photometric instrumentation is to relate the measured quantities to those characteristics of the ionosphere and auroral precipitation which may be derived or inferred from the basic measurements. This is done in Table 7. It should be noted at this point, that special effort has been made to cross-calibrate the photometric quantities with their equivalents as measured by the incoherent scatter radar. By this endeavor, we have made both radar and photometric data more useful, and more believable with respect to presenting a true picture of auroral-ionospheric conditions.

3.3 FIELD WIDENED INTERFEROMETER ROCKET EXPERIMENT

3.3.1 Experimental Plan

Ground-based optical support was provided to the DNA/AFGL Field Widened Interferometer (FWI), launched from Poker Flat at 0855UT, 13 November 1977, according to the experimental plan described in this section.

Table 7. Ionospheric irregularities: photometrically measured, and inferred quantities.

MEASURED QUANTITIES				
(A)	Photometric intensities versus time in same field-of-view			
	(1)	427.8 nm	N_2^+	E-region
	(2)	486.1 nm	H	E-region
	(3)	557.7 nm	O (1S)	E-region
	(4)	630.0 nm	O (1D)	E & F region
(B)	Photometric intensities versus time in three closely spaced fields of view			
	(1)	427.8 nm	N_2^+	E-region
	(2)	557.7 nm	O (1S)	E-region
	(3)	589.0 nm	Na	E-region
	(4)	630.0 nm	O (1D)	E & F region
	(5)	770.0–810.0 nm	OH	D-region

DERIVED QUANTITIES		
(C)	Energy deposit by precipitating particles (total)	from A1
(D)	Flux of precipitating protons	from A2
(E)	Photometric intensity ratios	from A4, A1
(F)	Auto and cross spectra and related statistical quantities	from B
(G)	Horizontal phase velocity of motions of emission irregularities	from F
INFERRED QUANTITIES		
(H)	Mean energy parameter of precipitating electrons	from E
(I)	Oxygen excitation and quenching chemistry kinetics	from A3, A4, E, F
(J)	Spatial structure of optical irregularities	from F
(K)	Auroral electric fields	from G, (B1, B2)
(L)	Pederson and Hall conductivities	from C, D, E
(M)	Joule heating in auroral regions	from C, E, K
(N)	Neutral winds and wavelike motions	from F, G
(O)	Frequency spectra of auroral E fields	from G
(P)	Large scale F-region structure	from A4

Three photometers were operated at the LMSC Chatanika optical site; two three-beam photometers and the meridional scanning trichroic photometer. The site was manned during every night of the rocket launch window, and instrumentation was operated from local dusk on every night that weather permitted. As in past operations, considerable background data were obtained for both quiet and active auroral conditions. These data will be useful in placing the FWI interferometer experiment in context of the types of auroral conditions as well as providing the requisite time history of auroral conditions before rocket launch. However, as practiced in the past support efforts, only a very limited amount of data will be looked at in detail.

Operation of the individual instruments and the data obtained are provided in Table 8. Support was also provided for WIDEBAND satellite passes which required observation of F-region irregularities and their motions. Hence, 3B2 was operated at 630.0 nm wavelength rather than at 589.0 nm or 770.0 nm as suggested in the original experimental plan.

It should be noted that the rocket launch was conducted under less than satisfactory optical observing conditions: thin and variable haze conditions were present at Chatanika. Thus, care must be taken if detailed quantitative interpretations are to be made of the data presented herein, without further effort to separate local meteorological effects from the auroral phenomena observed.

3.3.2 Data Summary

Digital photon counting data from the three photometers operated in support of the Field Widened Interferometer rocket experiment were processed and examined to determine the proper operation of each photometer. The raw data counts for the interval surrounding the rocket launch are illustrated in Figure 11 for the multispectral photometer and in Figure 12 for the three-beam photometers.

The multispectral photometer (MSP) was operated in the meridional scan mode with a scan period (N-S-N) of 160 s. Examination of the data pattern in Figure 11 shows the presence of auroral emission somewhat to the north of zenith. Also shown are the dark current and calibration intervals recorded just before and just after the

Table 8. FWI experiment: ground optics support plan.

Three-Beam Photometer: No. 1

Wavelength:	557.7 nm
Observation:	Auroral motions
Data Output:	Auroral E-fields and Joule energy deposit in vicinity of rocket upleg. Also spatial structure of auroral precipitation.

Three-Beam Photometer: No. 2

Wavelength:	630.0 nm
Observation:	F-region motions
Data Output:	Scale sizes and drift velocity in the F-region

Trichroic Photometer

Wavelengths:	427.8 nm, 557.7 nm, 630.0 nm
Observations:	Meridional scan mode of intensity versus latitude (zenith angle)
Data Output:	Precipitation auroral electron energy deposit versus latitude and time (427.8 nm) Energy parameter versus latitude and time (ratio of 630.0 to 427.8 nm)

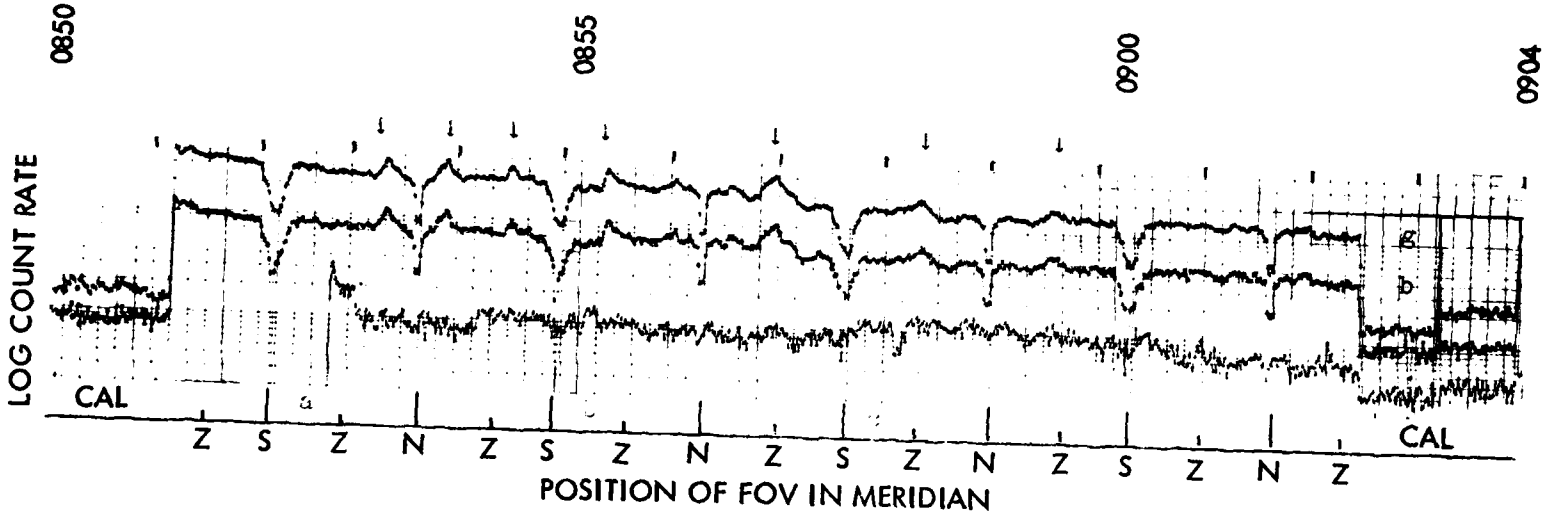

Figure 11. Raw data plot for meridional scanning multispectral photometer. Top scale indicates Universal time and position of arcs. Bottom scale indicates pointing direction from 10° elevation angle from southern horizon (S) to 10° elevation angle from northern horizon (N). Letters a, b, c indicate scans for which calibration plots were made for this report. Plot g is for 557.7 nm intensity, plot b is for 427.8 nm intensity. Other line is for 630.0 nm channel which was inoperative.

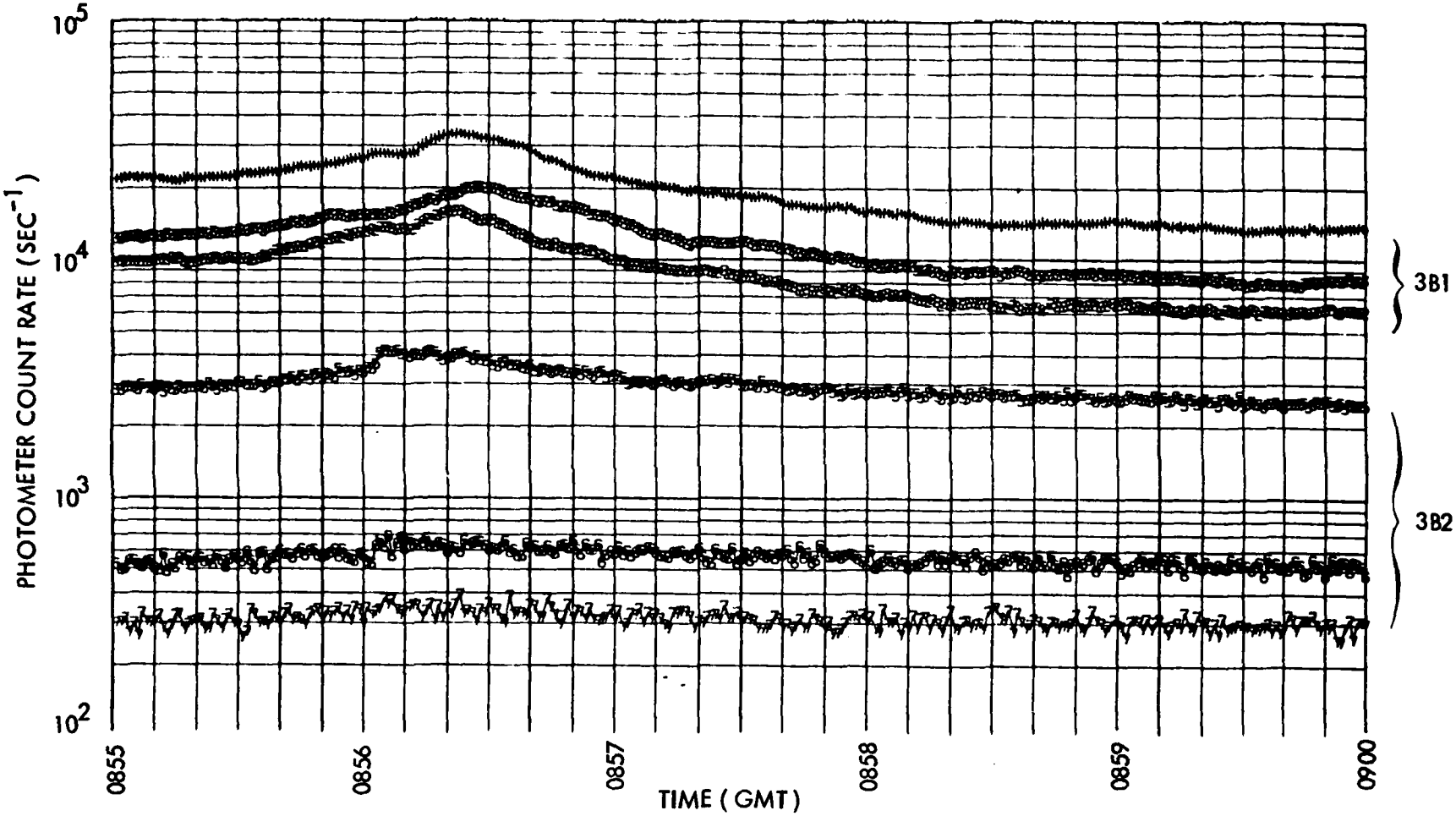

Figure 12. Three-beam photometer counting rates during period of Field Widened Rocket launch. Channel identification is: 2, 3B1-N; 3, 3B1-E; 4, 3B1-W; 5, 3B2-N; 6, 3B2-E; 7, 3B2-W. Photometer 3B1 operating at 557.7 nm, 3B2 operating at 630.0 nm.

FWI experiment. The MSP channels in blue (427.8 nm) and green (557.7 nm) appear to be operating correctly over the period of the rocket experiment, but the red channel (630.0 nm) appears to be degraded in response. Examination of the analog record which was made simultaneously with the digital record also shows this problem. Further analysis of these data probably will be limited to the green and blue channels.

The three-Beam photometers (3B) were operated on two different wavelengths. 3BP1 operated on 557.7 nm in order to monitor auroral motions, whereas 3BP2 operated on 630.0 nm in order to monitor the response of the F-region auroral emission. The difference between the two sets of data then may be used to infer the motions of the neutral species in the F-region after proper analysis.

The three-beam photometer data are illustrated in Figure 12. A single 5-min data segment is shown for the period of the FWI rocket flight. During the flight, the auroral arc appeared to peak in intensity just as it reached zenith at about 0855:30UT. The decrease in observed intensity after that time may have been due to increased haziness for a short period of time, or a real effect in the arc. The time delay observed between the three different photometer fields-of-view implies that the arc was moving in a generally northwest to southeast direction with a velocity of nearly 1 km/s. No corresponding clearcut auroral motion can be inferred from the second three-beam photometer data (3BP2) plotted in channels 5–7. The general haziness coupled with the weaker 630.0 nm emission intensity precludes direct interpretation of the raw data with confidence. Statistical processing of these data to determine the wavelike properties of the auroral motions is discussed in a later section.

3.3.3 Calibrated Scanning Photometer Data

The meridional scanning photometer operated properly on the 557.7 nm, green, and 427.8 nm, blue, channels. From these data one may infer the latitudinal distribution of energy input from precipitating auroral electrons during the FEI rocket experiment. In addition, some information may be derived on the mean energy parameter of the precipitating particles from the ratio of the two emission intensities. It should be noted, however, that these data must be viewed with caution because of the hazy

conditions present during the rocket launch period. The absolute intensity, energy deposit, and energy parameter values may be significantly affected by haze attenuation; therefore, these data should be taken as indicative of the auroral conditions rather than as absolute quantities.

The scanning photometer data were calibrated using the NUCAL code and several individual scans are plotted in Figure 13. Here, the photometric intensities and total energy deposited versus zenith angle (and distance from Chatanika) are plotted for a number of scans covering the rocket flight interval.

3.3.4 Multibeam Photometer Results: Auroral Motions and E-Fields

Statistical analysis of the three-beam photometer data was undertaken using the NUWAV code. The data from 3BP1 is directly related to the horizontal motion of the auroral emission pattern, hence, is interpretable in terms of motions of the structure in the precipitating particle flux. These results form a particularly good example of the quantities which can be inferred from the analysis. Figure 14 shows the power spectral densities computed for the intensity fluctuations in each of the photometer beams. The dispersion plot of auroral intensity fluctuation horizontal trace velocity is illustrated in Figure 15. Here we see velocity dispersion over a factor of 3 or more in the long-wavelength, low-frequency spectral range. The mean velocity of about 1 km/s agrees reasonably well with that inferred directly from the raw data plots. The direction of the wavelike disturbances of auroral motion does not agree well with that inferred from the raw data. This apparent discrepancy will be looked into in more detail. As with the multispectral photometer, the effects of variable haze may have created interference to the measurement.

Electric fields were inferred from the auroral motion data for the period of the rocket flight. Utilizing the method previously described by Sears (Reference 5), the magnitude of the E-field inferred is approximately 50 mV/m, with the direction mainly in the NE quadrant.

In addition to the auroral motion data discussed above, we have run a number of additional 5 min data samples through the NUWAV code to obtain equivalent information

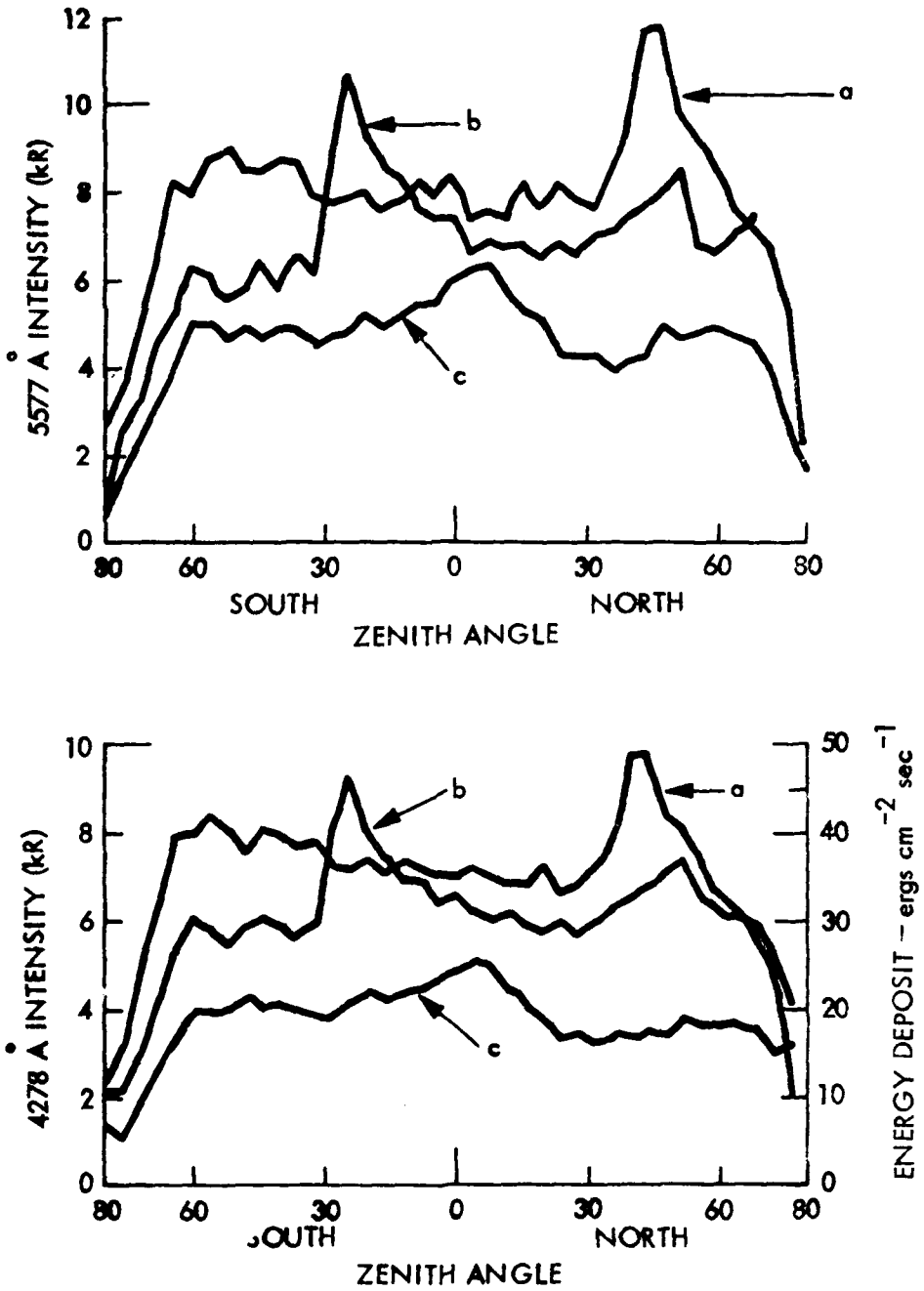

Figure 13. Calibrated scanning multispectral photometer data for 427.8 nm and 557.7 nm wavelengths. Three scans are plotted, beginning at times 0852, 0855, and 0858UT. The energy flux inferred from the 427.8 nm intensities is indicated as the right-hand scale on the 427.8 nm plot.

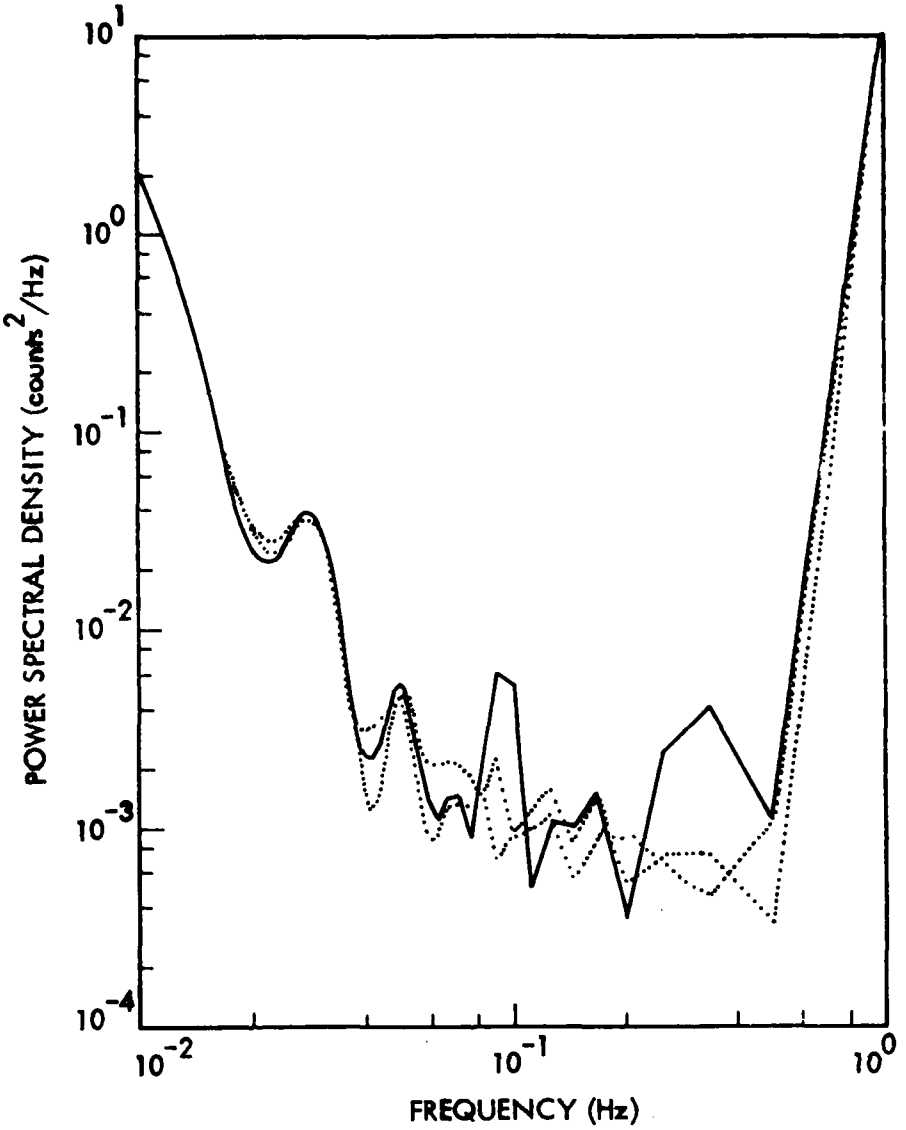

Figure 14. Power spectral density of 557.7 nm emission fluctuations observed with the multibeam photometer (3BP1). Each beam has a 1° FOV separated from its neighbors by 2°. Three plots presented correspond to PSD's measured in each photometer FOV.

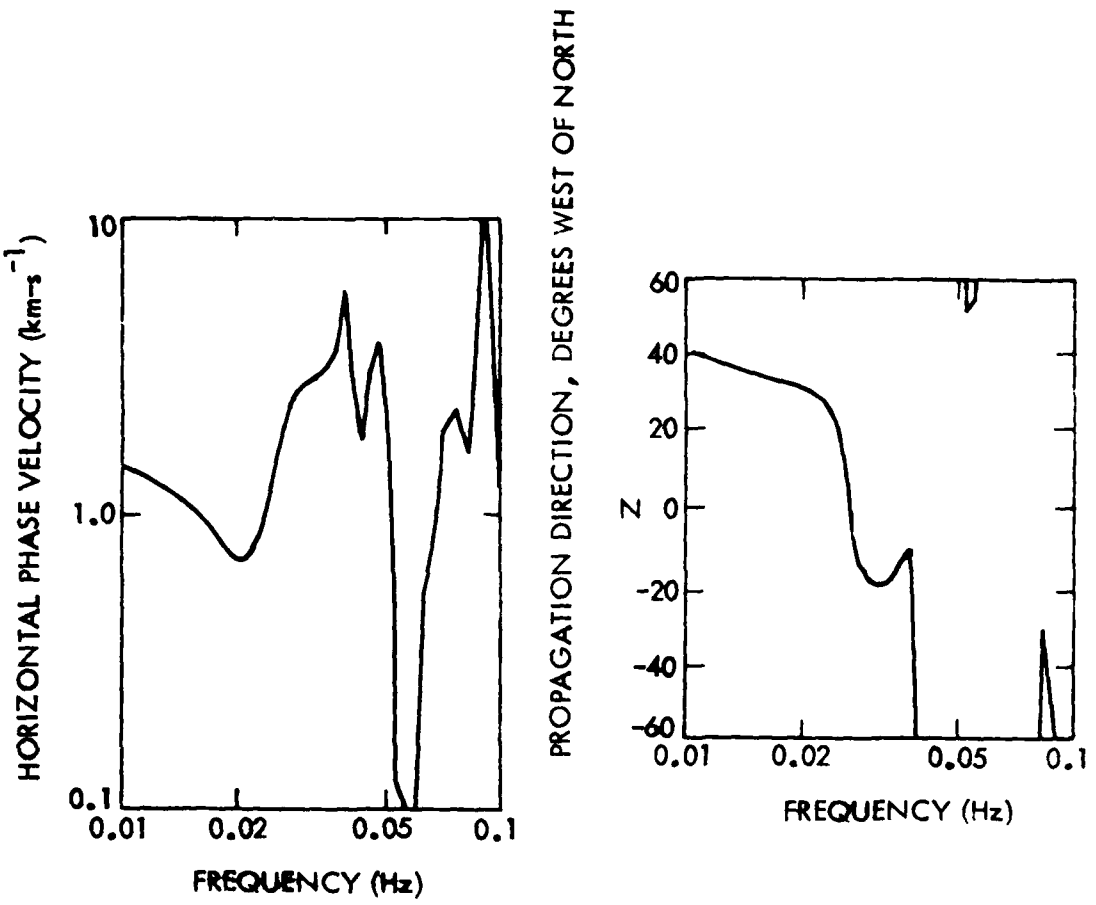

Figure 15. Horizontal phase velocity spectrum for 557.7 nm auoral motions. Note strong dispersion in magnitude and direction of velocity vector versus frequency measurement. Variability of velocity and direction above about 0.04 Hz is probably due to noise.

of auroral motions, E-fields, etc., over a longer period of time following the rocket shot. These data may be analyzed later in support of WIDEBAND pass studies conducted at SRI.

The multibeam data from 3B2 were processed in an identical manner as from 3B1 to obtain horizontal velocity spectra for the F-region. Figures 16 and 17 illustrate these data. As with the E-region auroral motion results, we see a generally high velocity around 1 km/s which shows dispersive properties. Because the average velocity and direction are nearly the same as the auroral motion data, we estimate that most of the F-region, 630.0 nm emission motion observed at the lowest frequency 0.01 Hz is due to direct auroral excitation with possibly some effects from neutral motions in the F-region as the frequency increases. A qualitative interpretation of the auroral motion and F-region motion data is that the F-region winds are moving in a southwesterly direction at a velocity of a few hundred m/s at this time.

3.3.5 FWI Photometric Data Summary

Scanning photometer and multiple beam photometer data were obtained in support of the FWI rocket experiment from which characteristics of the auroral energy deposit versus latitude and the magnitude and direction of auroral motions were determined. The three-beam photometer data supplied useful information on the temporal PSDs for the precipitating electron flux irregularities, ionospheric electric fields, and on the F-region temporal PSDs for the interval surrounding the rocket experiment. These data will be subjected to further analysis and submitted to the FWI rocket experiments as their requirements indicate.

3.4 WIDEBAND MULTI SUPPORT

3.4.1 Experimental Plan

The WIDEBAND MULTI (WBM) rocket was launched at 0811UT, 28 February 1978. The experimental plan for ground-based photometric support consisted of three

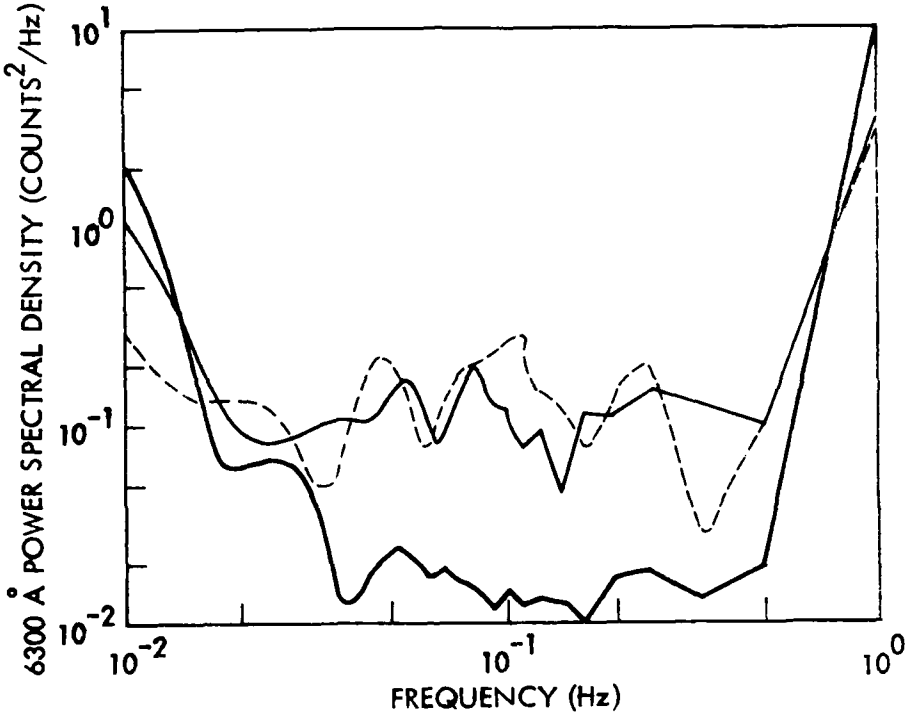

Figure 16. Power spectral density of 630.0 nm auroral F-region emission fluctuations measured with multibeam photometer (3B2). Dynamical range of fluctuation spectrum is reduced from that for 557.7 nm (Figure 14) because of lower signal-to-noise ratio. Otherwise, spectrum appears similar to that caused by purely auroral excitation fluctuations. Three plots presented correspond to PSD's measured in each photometer FOV.

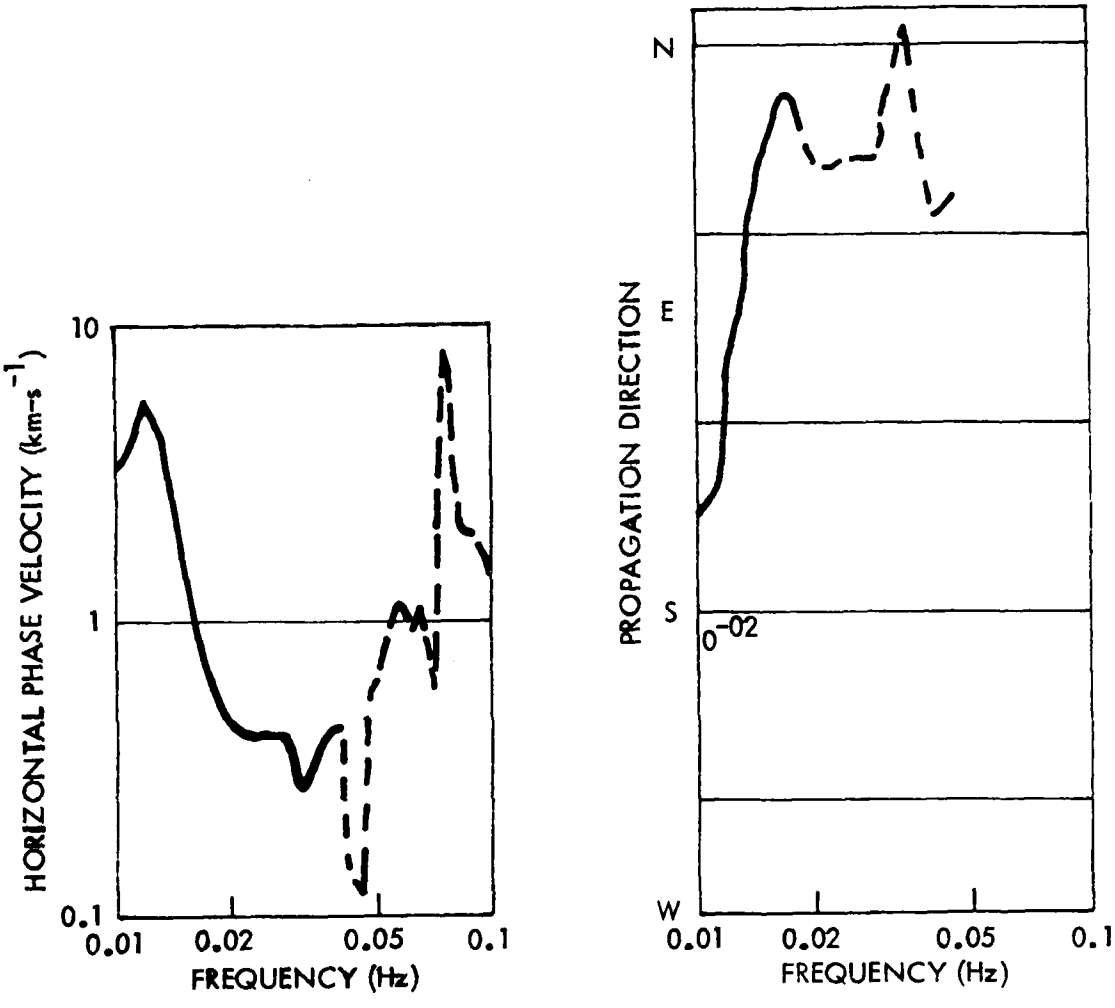

Figure 17. Horizontal phase velocity spectrum of 630.0 nm emission fluctuations. Note strong dispersion as in Figure 14, but with different directionality. Irregular character of plots at frequencies above about 0.04 Hz is due to noise.

main elements; definition of auroral input energy parameters and of ionospheric response to the aurora by means of the meridional scanning multiple color photometer; definition of the auroral scale sizes, motions, and inferred ionospheric electric fields by means of the 3B1 photometer operating on 557.7 nm; and definition of the F-region response, motions, and scale sizes by means of the 3B2 photometer operating on 630.0 nm wavelength. The experimental plan was essentially the same as that used for the Field Widened Interferometer experiment which is described in section 3.3.1.

3.4.2 Summary of Auroral Conditions

The WBM experiment was conducted during a period of intense and active auroral conditions. In the several hours prior to launch, a number of very intense, multiple arc systems developed, underwent poleward expansion and breakup, and subsequently reformed. At several times throughout the evening auroral conditions exceeded IBC III, consequently producing massive and continued ionization and infrared excitation sources. Auroral conditions during the 10-min period immediately prior to rocket launch and throughout the rocket flight are displayed in the scanning photometer data plot in Figure 18. At 0758UT, a poleward expansion and breakup took place, with subsequent fading and reformation of the auroral arc system. The dynamical nature of the widespread activity is exemplified in Figure 18 by the observation of rapid formation, motion, and dissolution of auroral forms from scan to scan, each of which takes 80 s to cover the meridian from north to south horizon. The three-beam photometer data which are illustrated in Figure 19 also shows the dynamical behavior of the aurora during this period.

3.4.3 Calibrated Auroral Intensities and Ionospheric Parameters

The CONX code was used to derive the auroral energy deposit and mean energy parameters as well as the ionospheric integrated Hall and Pederson conductivities versus distance from the zenith point at Chatanika. These data were derived from the calibrated meridianal scanning photometric intensity data, and correspond to the

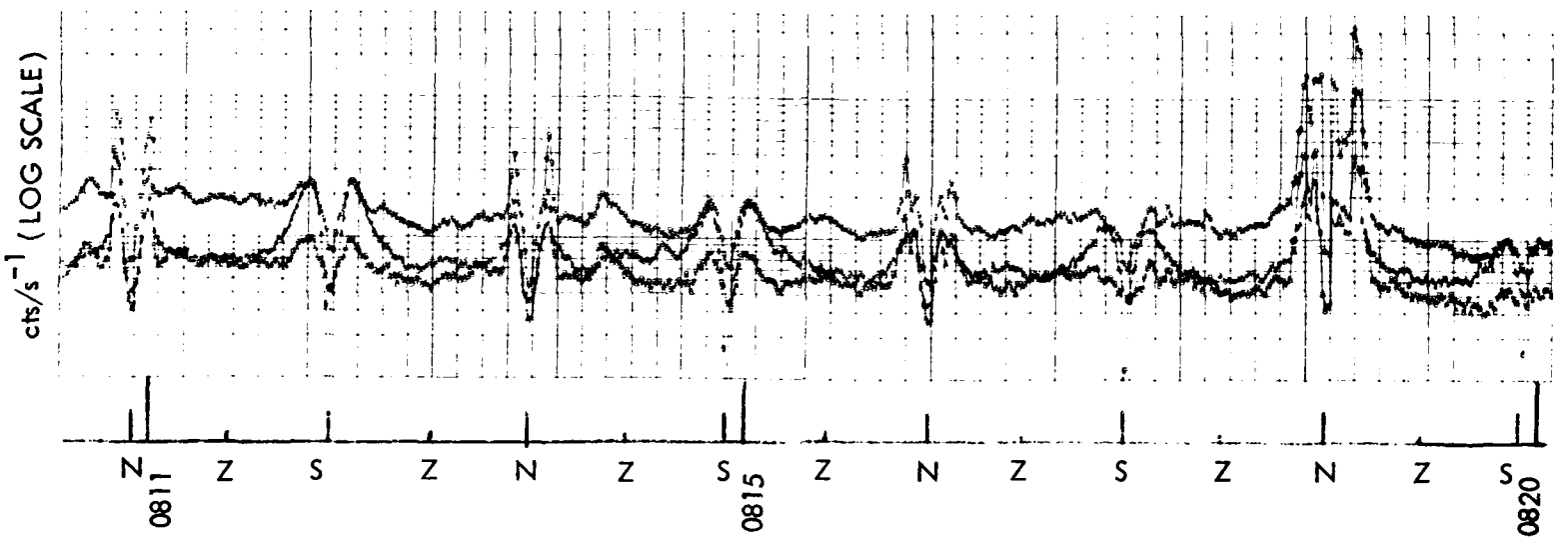

Figure 18. Data plot for 10-min period surrounding WIDEBAND MULTI rocket experiment 28 February 1978. Channel identification is: 8 – 557.7 nm ; 9 – 427.8 nm ; a – 630.0 nm.

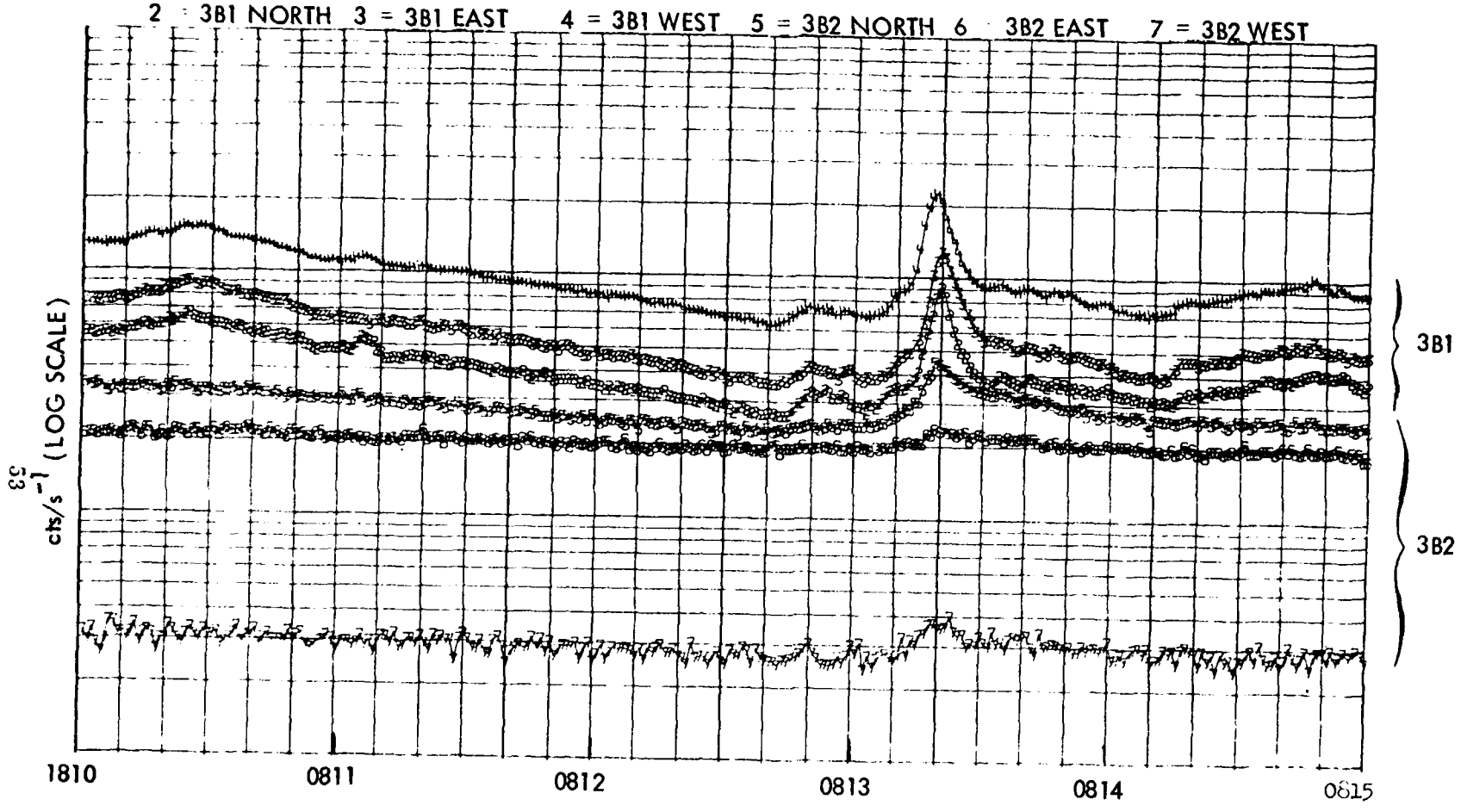

Figure 19. Three-beam photometer data plot for 0810 to 0815UT period during WIDEBAND MULTI rocket experiment, 28 February 1978. Photometer 3B1 operated on 557.7 nm : photometer 3B2 operated on 630.0 nm.

interval most closely covering the rocket flight, i.e., 0808:15UT through 0820:15UT. Nine complete horizon-to-horizon scans are presented.

Examination of the plots of total energy deposited in the atmosphere versus distance from Chatanika as illustrated in Figure 20 shows that the activity near zenith and to the south decreased in overall intensity during the rocket experiment, although the total energy flux is still very high, ranging from about 25 to 50 ergs/cm^2-s. The auroral system approximately 200-km north of Chatanika faded briefly in the 4-min interval from 0812 to 1816, but then rapidly intensified to very large energy flux levels, exceeding 500 ergs/cm^2-s during one scan. The mean energy parameter, EBAR, also exhibited similar spatial and temporal behavior as the total energy, as illustrated in Figure 21. Immediately following the data segments shown and discussed here, a breakup occurred and the sky was once more covered by extremely intense and active forms.

The height-integrated ionospheric Hall and Pederson conductivities were extremely large during the period covering the WBM experiment, as might be expected from the particle energy deposit data. Hall and Pederson conductivity plots contained in Figures 22 and 23 show a general spatial and temporal variation consistent with those shown by the total energy and mean energy plots. Because the conductivity models did not extend over the range of very high mean energy parameter values observed during this aurora, many of the conductivity plot points are off-scale. Off-scale points are plotted on the x-axis but should be understood to refer to off-scale values greater than the maximum conductivity values on the abscissa.

To the extent that ionospheric conductivity may be related to the plasma processes which generate ionospheric striated irregularities, for example by the gradient drift instability mechanism, these conductivity data will provide valuable input to study of the generation of striated regions.

3.4.4 Auroral Motions and Electric Fields

Auroral motions were observed simultaneously in two wavelengths, 557.7 nm and 630.0 nm by the 3B1 and 3B2 photometers, respectively. Motions observed at 557.7 nm

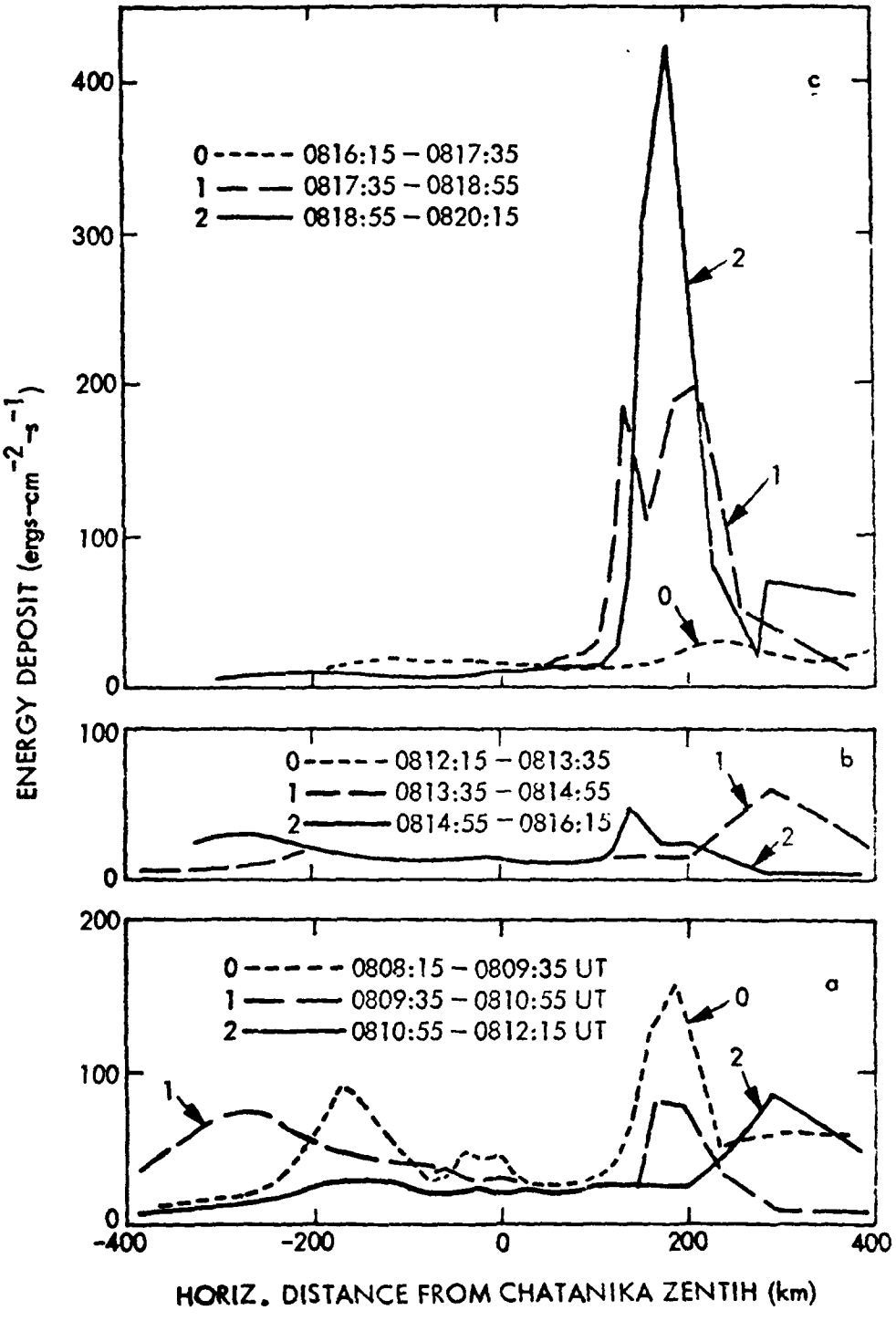

Figure 20. Total energy deposit versus distance from Chatanika for period of the WBM experiment, 20 February 1978. Each panel presents three consecutive scans of 80-s duration each. The total time period covered is 0808:15 to 0820:15UT.

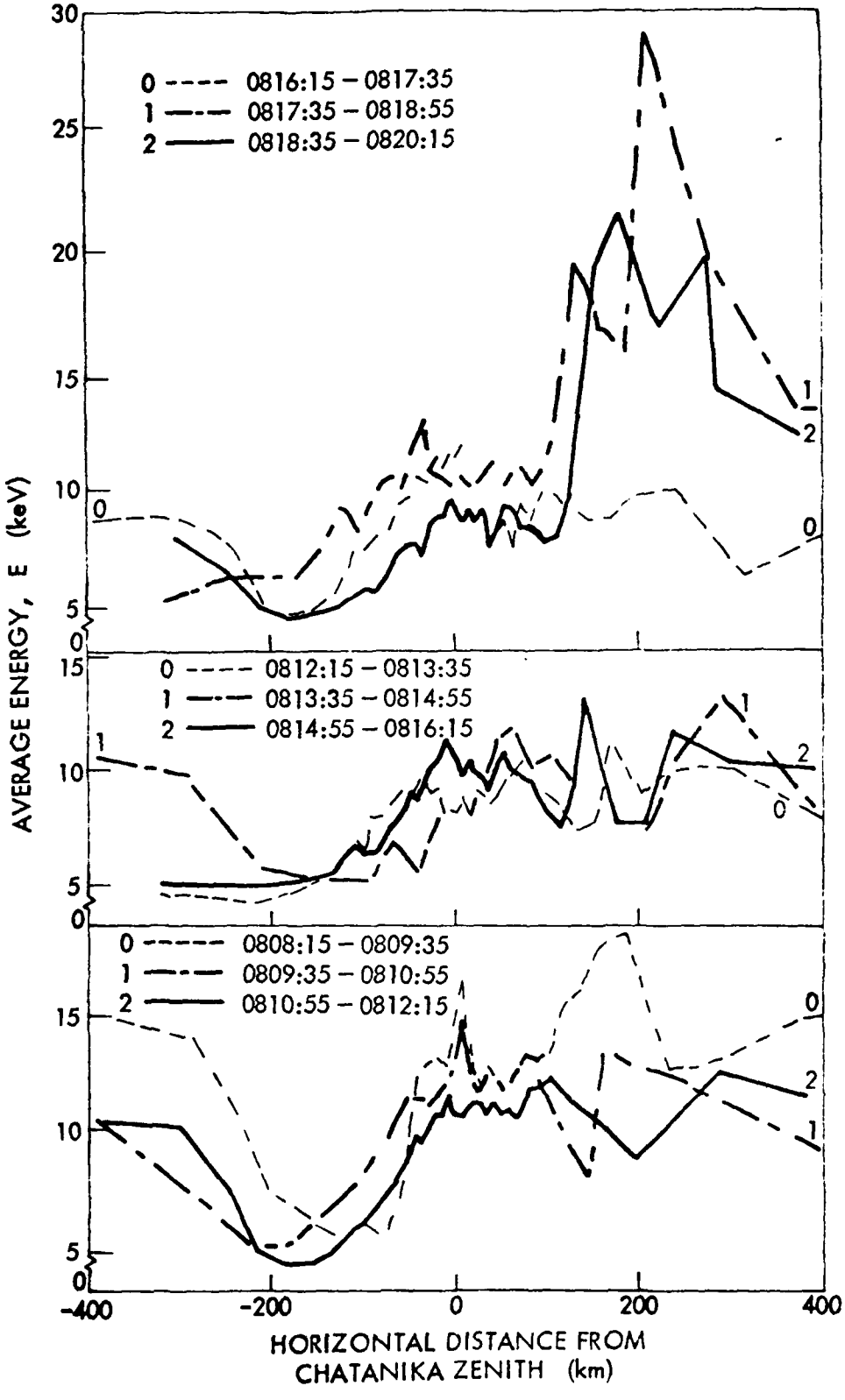

Figure 21. Average energy of precipitating electron flux plotted versus distance from Chatanika zenith. Each frame represents three scans of 80-s duration each during the WBM experimental period.

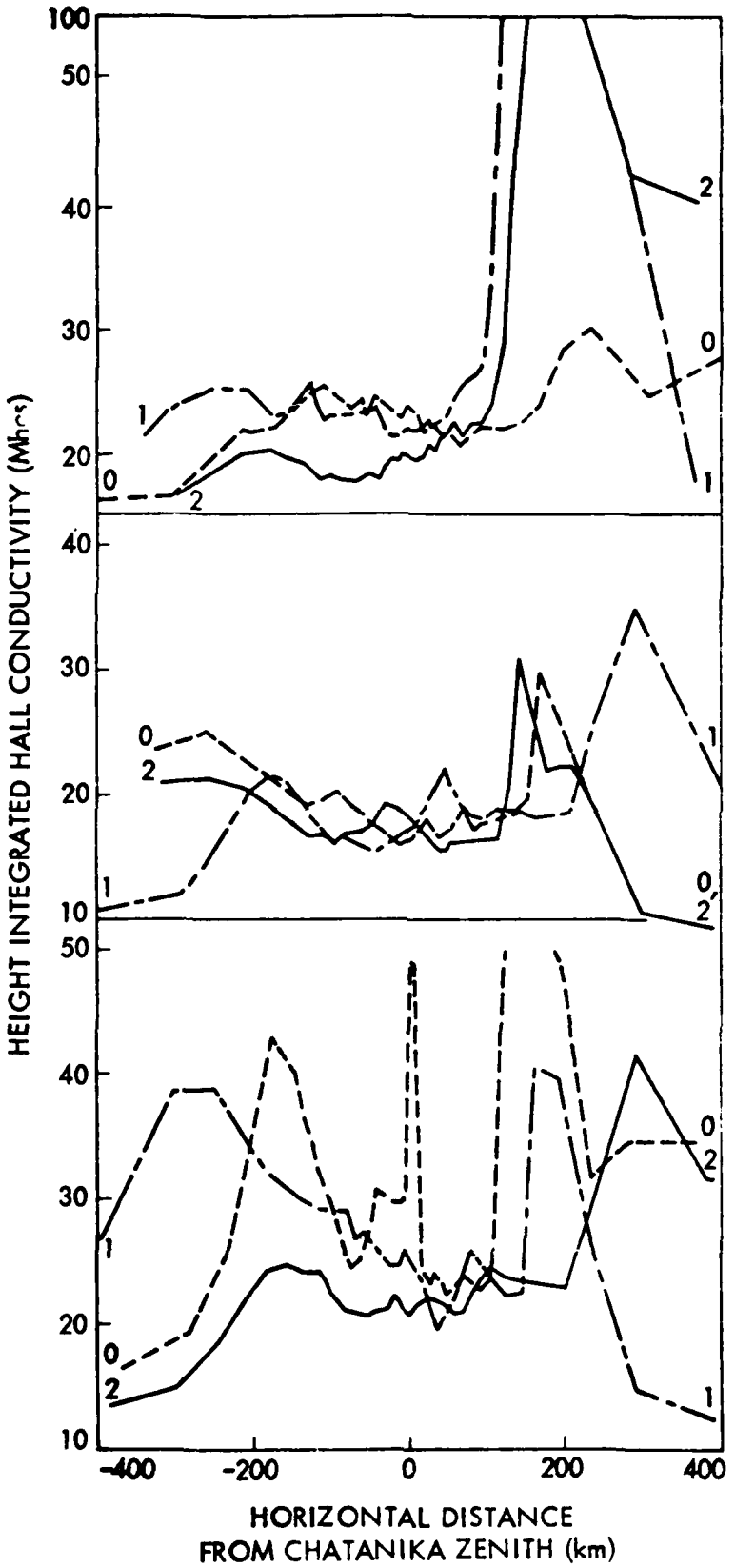

Figure 22. Plot of height-integrated Hall conductivities versus horizontal distance from Chatanika zenith during WBM experiment. Panels, and times are the same as Figures 20 and 21.

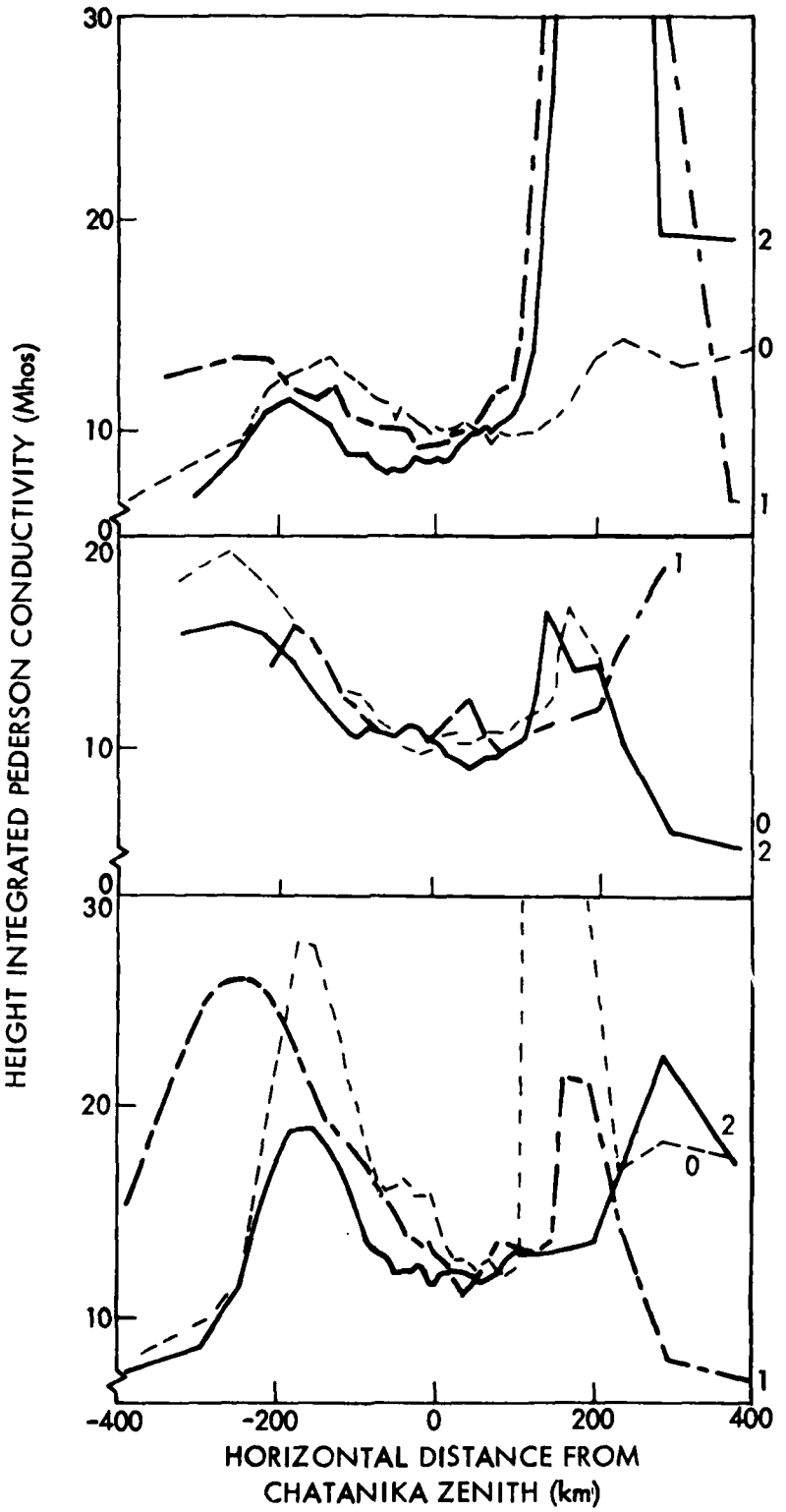

Figure 23. Plot of height-integrated Pederson conductivities versus horizontal distance from Chatanika zenith for WBM experiment. Panels and times are the same as in Figures 20, 23.

may generally be attributed to motions of the irregularities in the precipitating electron flux within the temporal resolution of the digital photon-counting system because the radiative lifetime of the 0 (^{1}S) state from which 557.7 nm emission originates is less than about 1 s. The altitude profile of 557.7 nm emission is mainly bounded by the E-region. Emission in the 630.0 nm spectral line [0 (^{1}S) - 0 (^{1}D)] is a more complicated function of auroral excitation and atmospheric response. In an undisturbed atmosphere, most of the 6300 A emission is confined to the F-region and has a radiative lifetime of 60 to 100 s. The 0(^{1}D) state is strongly quenched below about 200 km by collisions. Thus, motions observed in the 630.0 nm emission line reflect both the motions of the excitation source, e.g., precipitating electrons, and motions of the neutral, excited species in the atmosphere after excitation. In principal, it may be possible to unfold the two effects in order to derive the F-region (or upper E-region) neutral winds, but this has not been accomplished as yet.

In this section we present the results of interpretation of the 557.7 nm, 3B1, emission data in terms of auroral temporal and spatial PSDs and in terms of the ionospheric electric fields during a period including the WBM rocket experiment.

Temporal PSDs. Temporal PSDs were computed for the 557.7 nm data obtained using 3B1, over the interval 0745–0845UT. The code, NUWAV10 was used as described in this report. Figure 24 illustrates a matrix of temporal PSDs for this interval. All PSDs observed had a form $P = P_o f^{-n}$ where n ranges from about 1.5 to 2.5. Evidence exists in some of the frames for coherent modulation of the precipitating electron flux such as commonly occurs in pulsating auroras, but auroral conditions were generally so chaotic during this time interval that no significant intervals of coherent pulsations were observed by eye.

Spatial PSDs. Spatial PSDs were also computed for the same interval as the temporal PSDs. These results are illustrated in Figure 25 which contains the matrix of PSDs in the same format as those shown previously. As previously discussed in this report, the NUWAV code has not be optimized as yet to smooth the spatial PSD results; hence, we have performed an approximate smoothing of these data in order to obtain at least

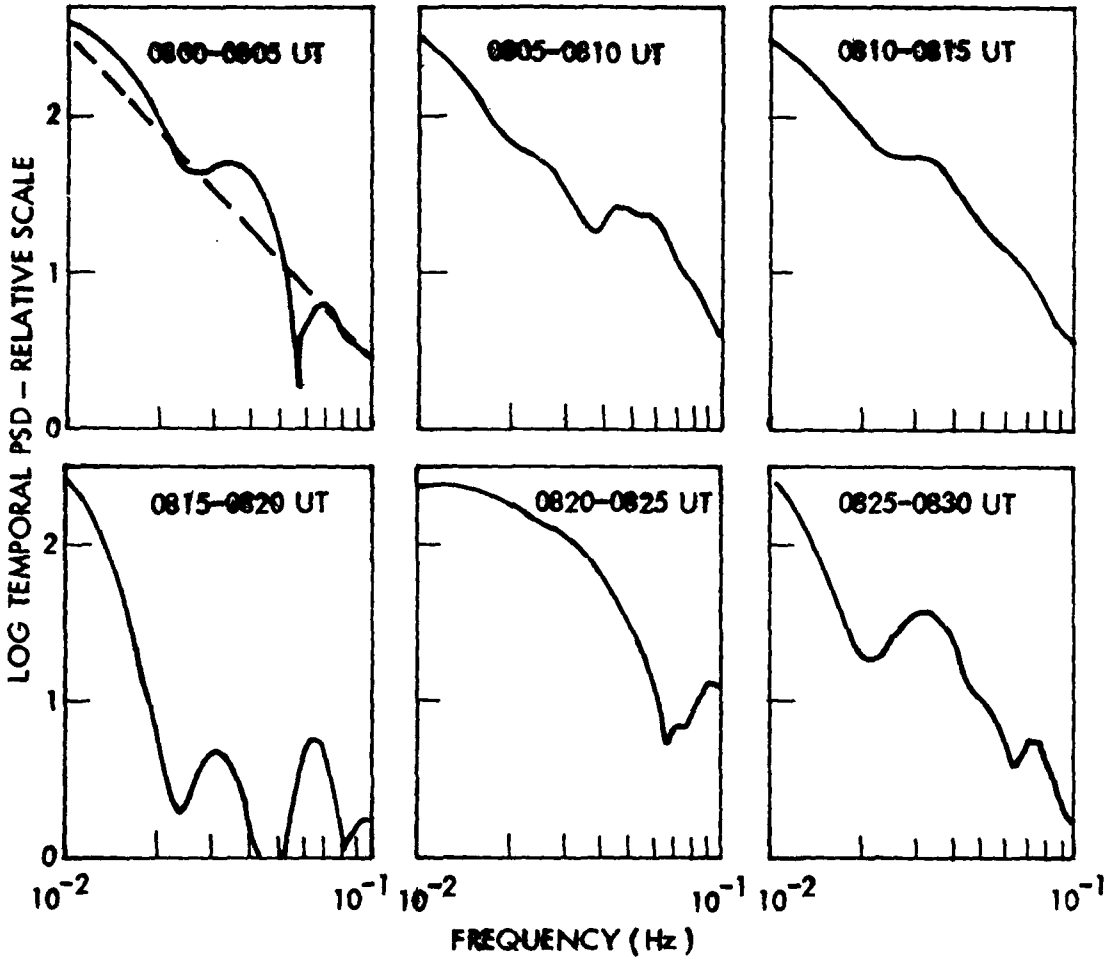

Figure 24. Temporal PSD matrix.

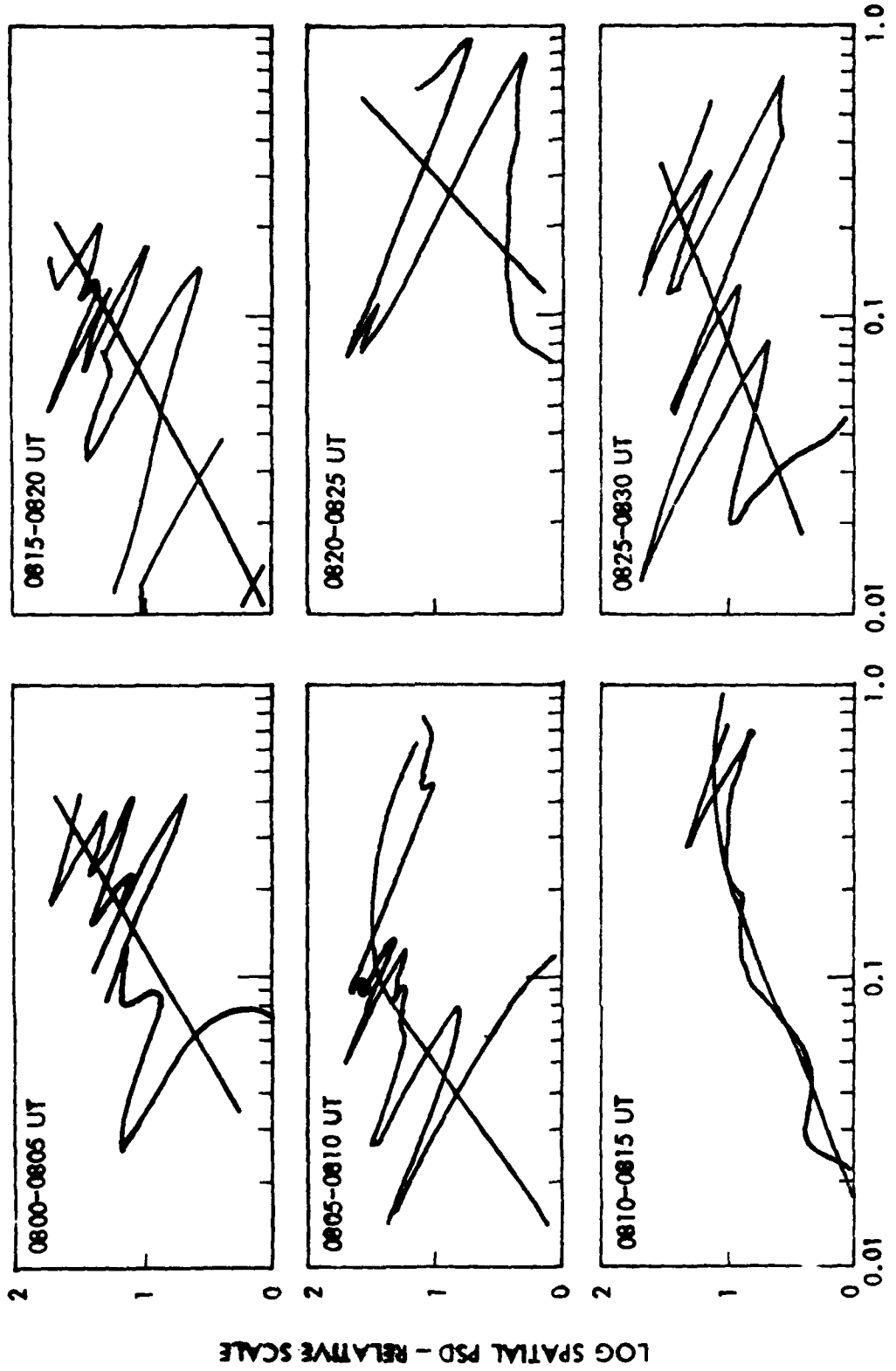

Figure 25. Spatial PSD matrix.

an approximate idea of the SPSD form. All of the SPSDs illustrated appear to be of the form $P = P_o k^n$ where n is generally between 0 and 1. There is some evidence for turnover of the spectrum at high spatial frequencies, thus indicating a change from the energy input spectrum (at low k) to the turbulent type spectrum (at high k).

Electric Fields. The ionospheric electric fields are inferred from the auroral velocity spectrum which is derived from the NUWAV code as illustrated in section 2.8 of this report. To infer electric fields, one must hypothesize that the auroral motions measured by the 3B photometers are entirely due to the ExB forces impressed upon the flux tubes containing the precipitating electron flux. Comparison of E-fields inferred from auroral motion data with those derived from ionospheric plasma motions as measured by the Chatanika incoherent scatter radar have generally agreed in qualitative behavior, but less good quantitative agreement has been attained as yet. It is believed that some of the quantitative differences between radar, E-fields and photometric E-fields are caused by the different fields-of-view and integration times inherent in the two instrumentation techniques. However, E-fields presented herein must be considered to be strictly an inferred quantity, which may disagree from other measures of E-fields either because of instrumentation artifacts or from the basic physical properties of the auroral ionospheres.

The inferred E-fields throughout the period of the WBM experiment are plotted in Figure 26. Here, we have adopted the minimum frequency value, i.e., the value of inverred E-field at the lowest frequency of the velocity spectrum. As discussed in previous reports on E-fields (Reference 11), this value typically represents that which would be obtained with a dc, or zero frequency measurement, and is usually the minimum E-field value (or velocity value) in the overall velocity dispersion plot. Comparison of E-field magnitudes against the intensity of auroral precipitation as illustrated by the calibrated total energy plots indicates that as the auroral intensity diminished just prior to the very intense arc enhancement at about 0816UT, the E-fields increased.

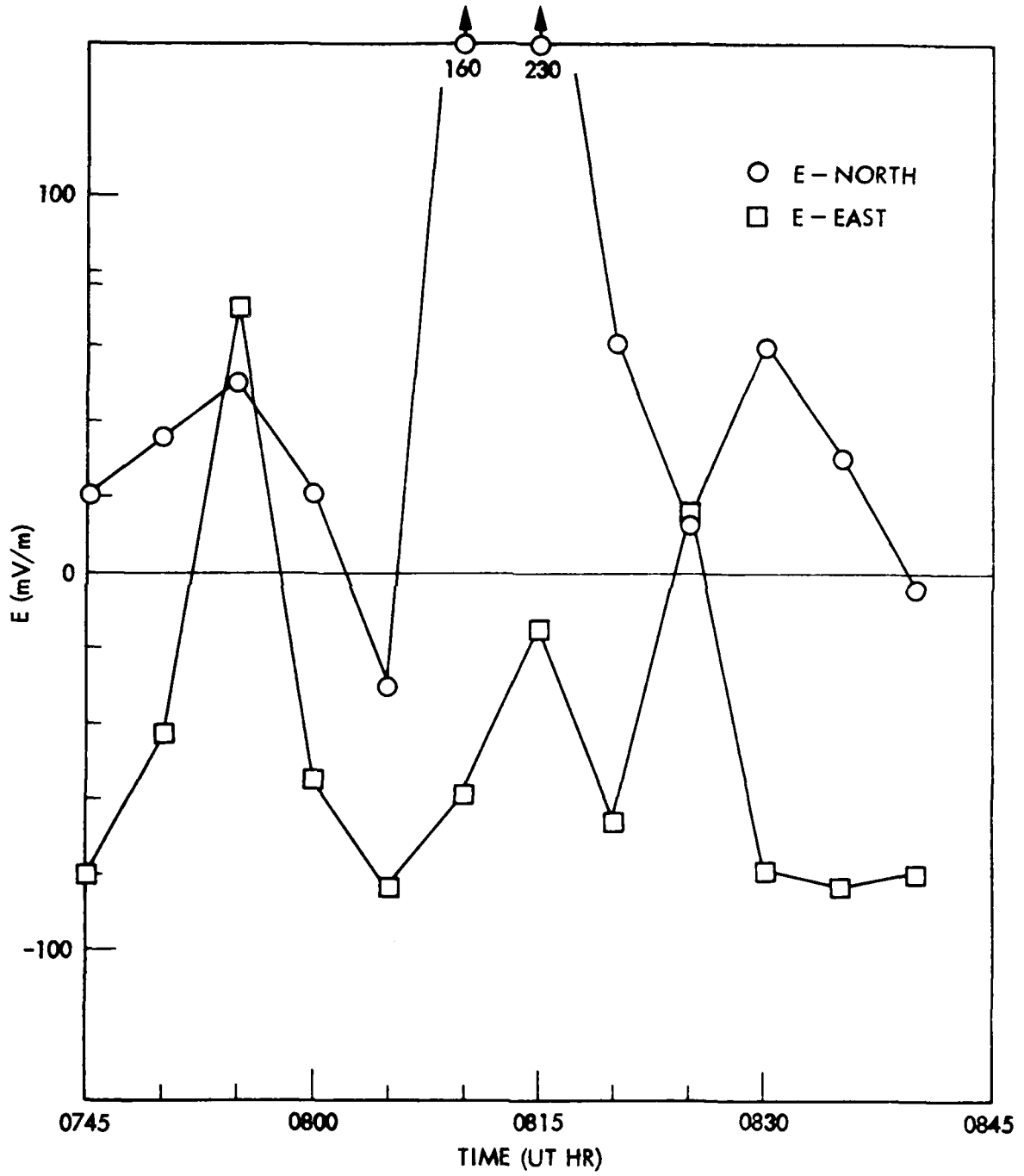

Figure 26. Estimates of auroral electric fields around time of WIDEBAND MULTI rocket experiment; 28 February 1978. These values inferred from large scale motions of aurora, observed with 3P1.

3.5 SWIR/SWIR/TMA SUPPORT

3.5.1 Experimental Plan

The SWIR/SWIR/TMA rocket experiment goals were to define the altitude and latitudinal extent of energy deposited in the atmosphere by a well-defined quiet auroral arc, and to measure the latitudinal extent of the infrared radiance in certain bands in comparison with the energy input distribution and its history. This experiment was undertaken because certain infrared active species participate in energy transfer reactions with atmospheric constituents which can provide an energy reservoir for IR emission. Transport of the excited but non radiative species by neutral winds can take place, thus spatially broadening the apparent radiance pattern of the IR emission as compared with the pattern of energy deposit.

The two SWIR rockets were intended to monitor the spatial extent of the IR emission by flying over and under the arc. The TMA release was intended to provide a neutral wind profile over the altitude range of interest, about 80 to 120 km.

To augment the original SWIR/SWIR/TMA experiment, an additional rocket payload intended to monitor the spatial variations in precipitating particle flux, hence energy deposit, was added to the program. This rocket provided useful total energy deposit data, through the arc, on a one time basis, which will be supplemented by the ground-based photometric data.

The ground-based support provided by the photometric measurements concentrated on definition of the energy deposit in the quiet arc from precipitating particles; determination of ionospheric electric fields which might affect the energy deposit in the vicinity of the arc, through Joule heating processes for example; and measurement of the neutral winds in the 96-km region using observations of the drift of the sodium airglow patterns. The latter measurement was to have been calibrated against the TMA trail. The experimental design of the ground-based photometric support measurements for this series of rocket experiments is summarized in Table 9.

Unfortunately, only one of the SWIR instruments was successfully launched, and the TMA trail failed to deploy. Thus, although the main goal of the experiment was

Table 9. SWIR/SWIR/TMA: ground optics support plan

Three-Beam Photometer: No. 1

Wavelength:	557.7 nm
Observation:	Auroral Motions
Data Output:	Auroral E-fields and Joule energy deposit in vicinity of rocket upleg. Also spatial structure of auroral precipitation

Three-Beam Photometer: No. 2

Wavelength:	589.0 nm
Observation:	D-region Atmospheric Motions
Data Output:	Scale sizes and drift velocity for neutral constituents in the D-region; to be cross calibrated by TMA trail data

Trichroic Photometer:

Wavelengths:	427.8 nm, 557.7 nm, 630.0 nm
Observations:	Meridional scan mode of intensity versus latitude (zenith angle)
Data Output:	Precipitation auroral electron energy deposit versus latitude and time (427.8 nm). Energy parameter versus latitude and time (ratio of 630.0 to 427.8 nm) and ionospheric conductivities versus distance from Chatanika

not realized, successful operation of one SWIR instrument will still enable a great degree of useful data to be obtained with highly useful results, especially when the rocket- and ground-based data are combined.

3.5.2 SWIR Experiment Data Summary

Ground-based photometric data were obtained in support of the SWIR experiment on the three-color photometer, operated in the normal meridional scan mode, and on three-beam photometer 3B1, operating on the 5890 A emission wavelength of Na. The additional photometer channels were assigned to the MTP instrument which was still undergoing tests, hence no data relating to auroral motions or electric fields were obtained.

The meridional scan data, illustrated in Figure 27, show a strong auroral arc, located just to the north of zenith. This arc persisted for many minutes prior to launch of the SWIR rocket, and was very stationary in its position. Thus it represents a strong, fairly constant source of excitation for the atmosphere in the 90- to 120-km altitude range of interest.

Data were obtained from the three-beam photometer 3B1 which monitored Na airglow emission and its horizontal motions; however, some extraneous noise appeared intermittently in the system and further examination of the data will be required in order to assess its usefulness.

3.5.3 Calibrated Meridional Photometer Data

The meridional scanning photometer data were calibrated using the CONX code which outputs both the calibrated photometric intensities, and their interpretation in terms of auroral parameters total energy deposit, mean energy parameter, ionospheric parameters, and height-integrated Hall and Pederson conductivities. These outputs are plotted versus distance from Chatanika in Figures 28 through 31. Three scans each of 80-s duration are plotted in each figure representing the arc and ionospheric parameters during most of the rocket flight. The initial scan began approximately at rocket launch time, 0914UT.

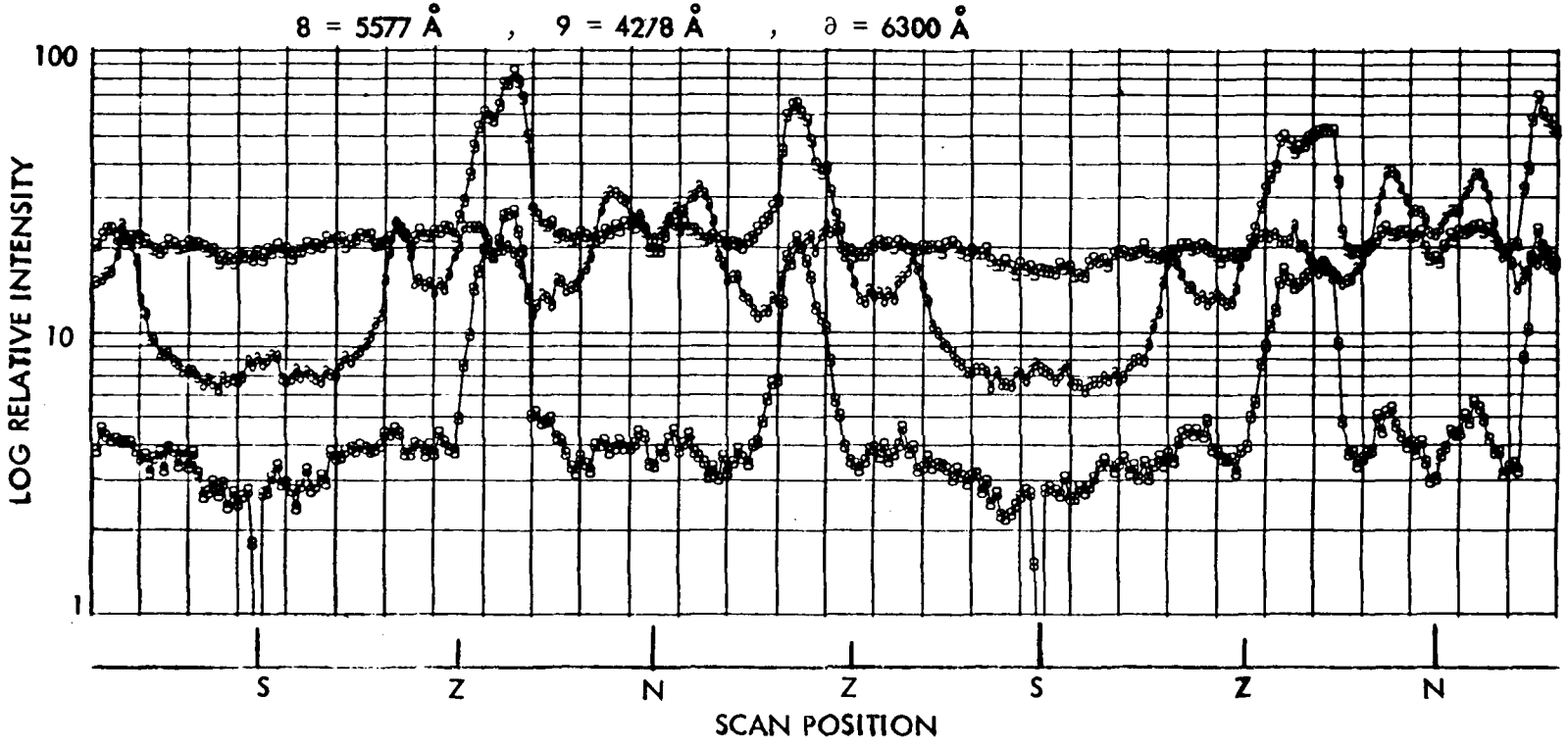

Figure 27. Three-color scanning photometer data for period of SWIR launch on 26 October 1978. Data segment extends from 0910:52 through 0915:51UT. Note intense arc just to the north of zenith (Z) with apparently less energetic structure both to the north and south. Each N-S scan requires 80 s.

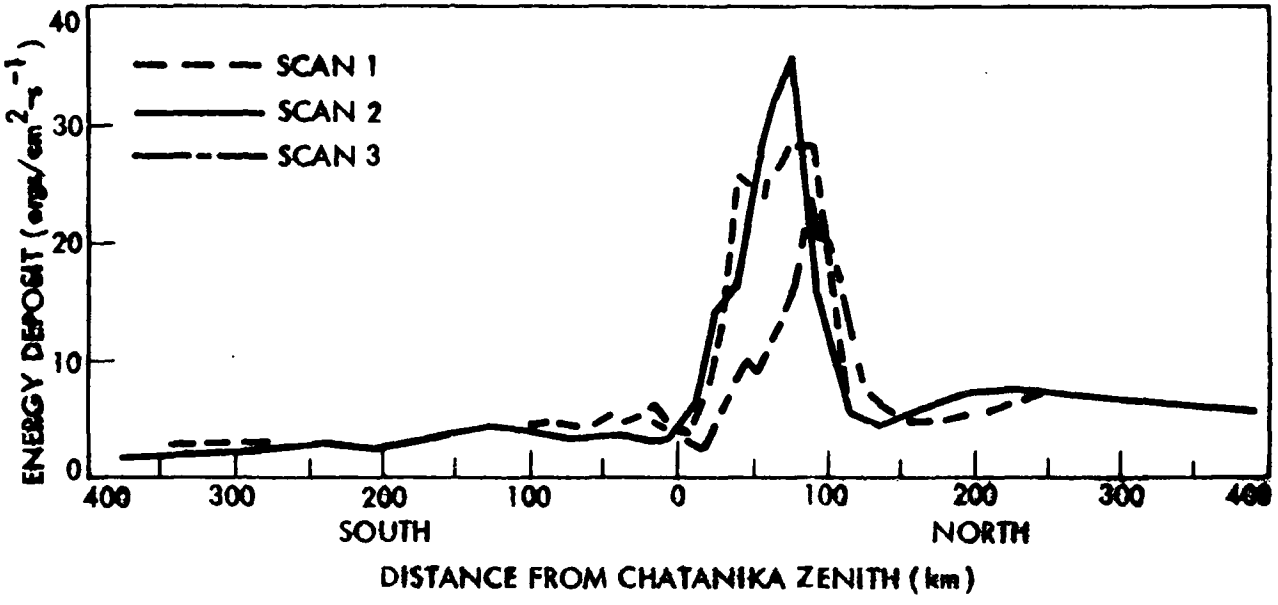

Figure 28. Total energy deposited in the ionosphere versus distance from Chatanika zenith for period of SWIR rocket experiment on 26 October 1978. Each scan is of 80 seconds duration, with the first scan commencing at rocket launch time, 0914 UT.

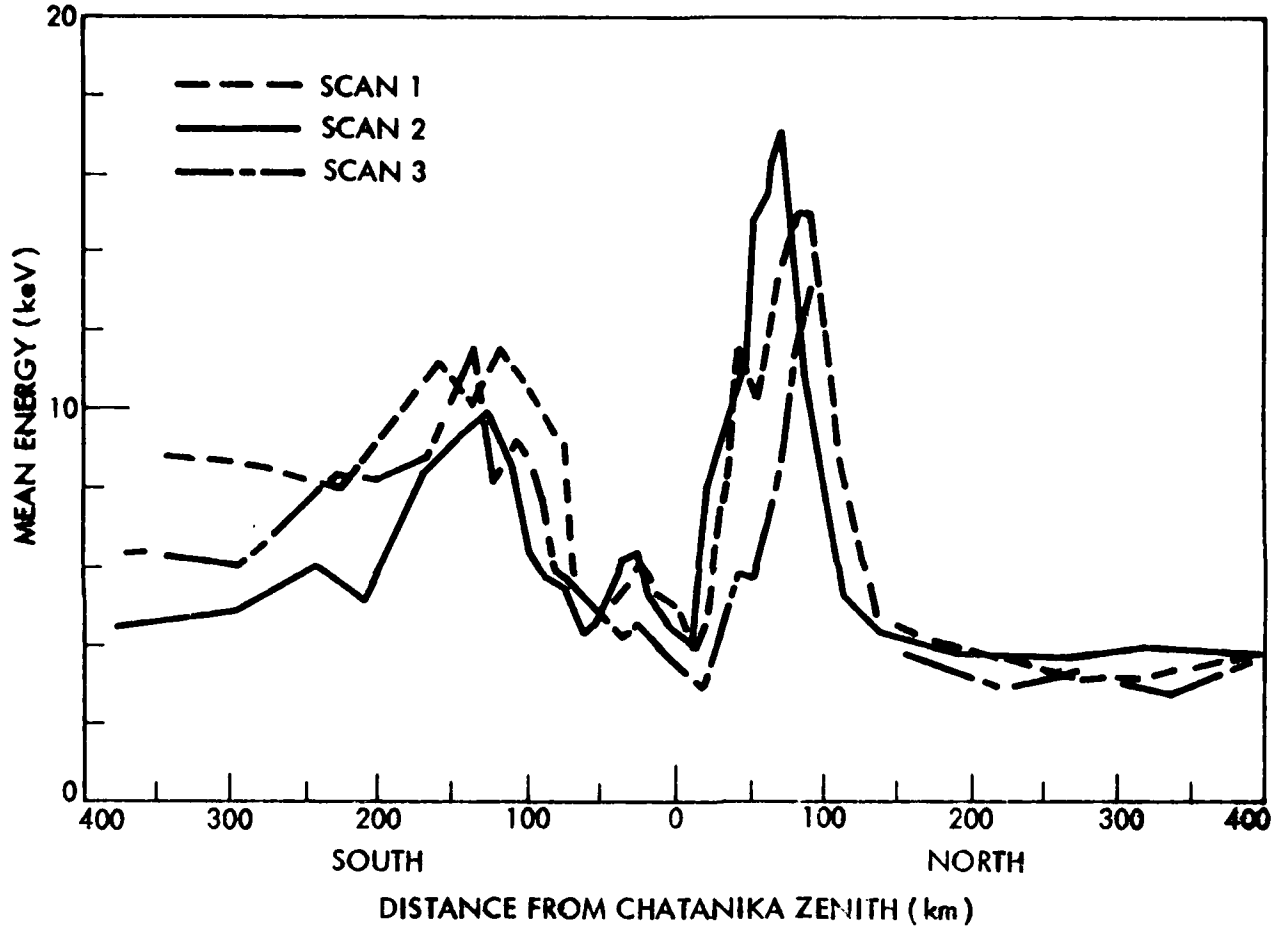

Figure 29. Mean energy parameter for precipitating electrons during SWIR launch, 26 October 1978. Note narrow, inverted V" energy enhancement in the arc located to the north of geographic zenith. Enhanced energy parameter values to south of zenith are probably due to scattered light from Fairbanks due to haze near southern horizon. Scan times are the same as Figure 28.

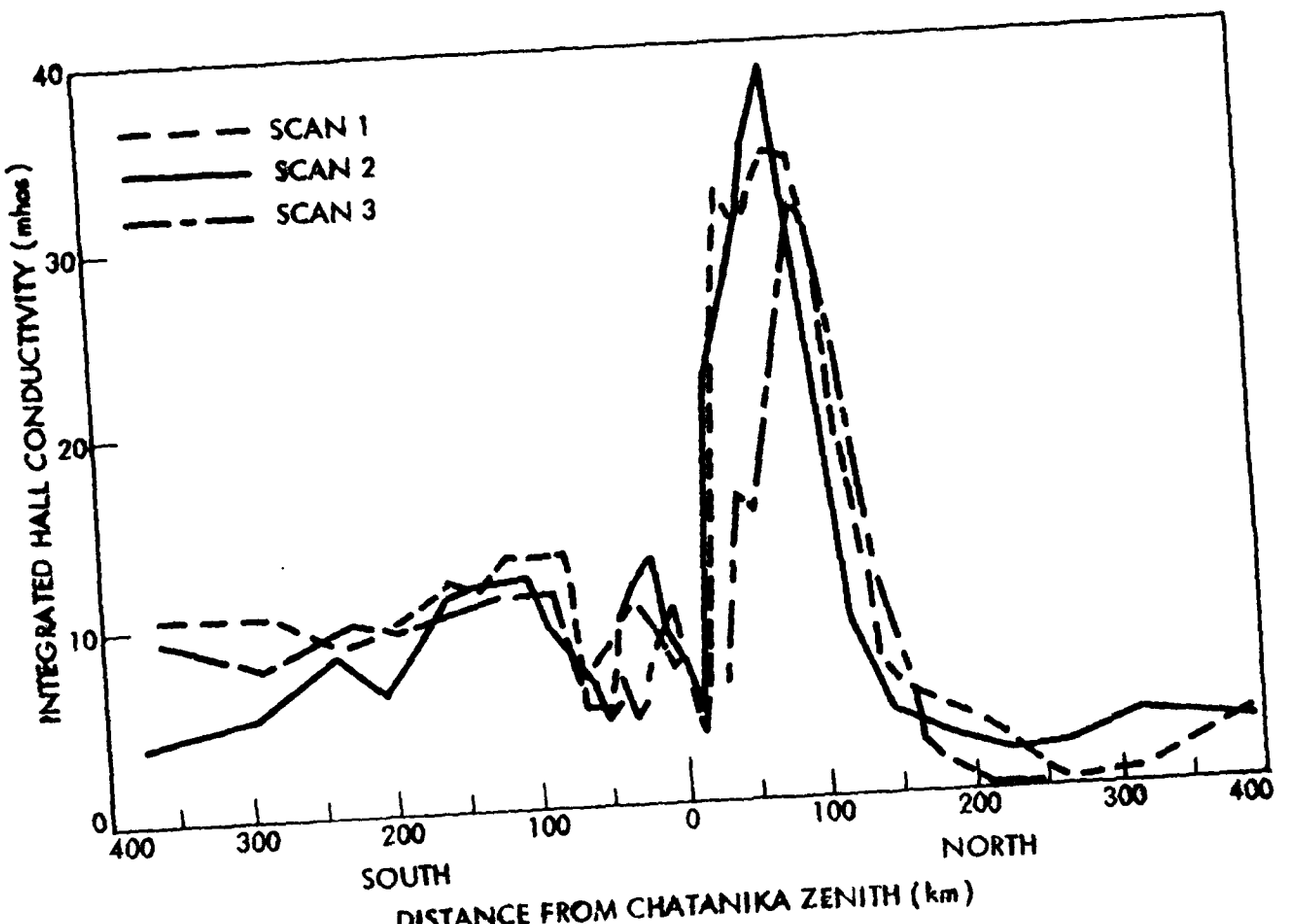

Figure 30. Height integrated Hall conductivity for period during SWIR launch, 26 October 1978. The assymetry in Hall conductivities to the north and south of the auroral arc is probably due to haze in the southern region, as described in Figure 29. Scan times are the same as Figure 28.

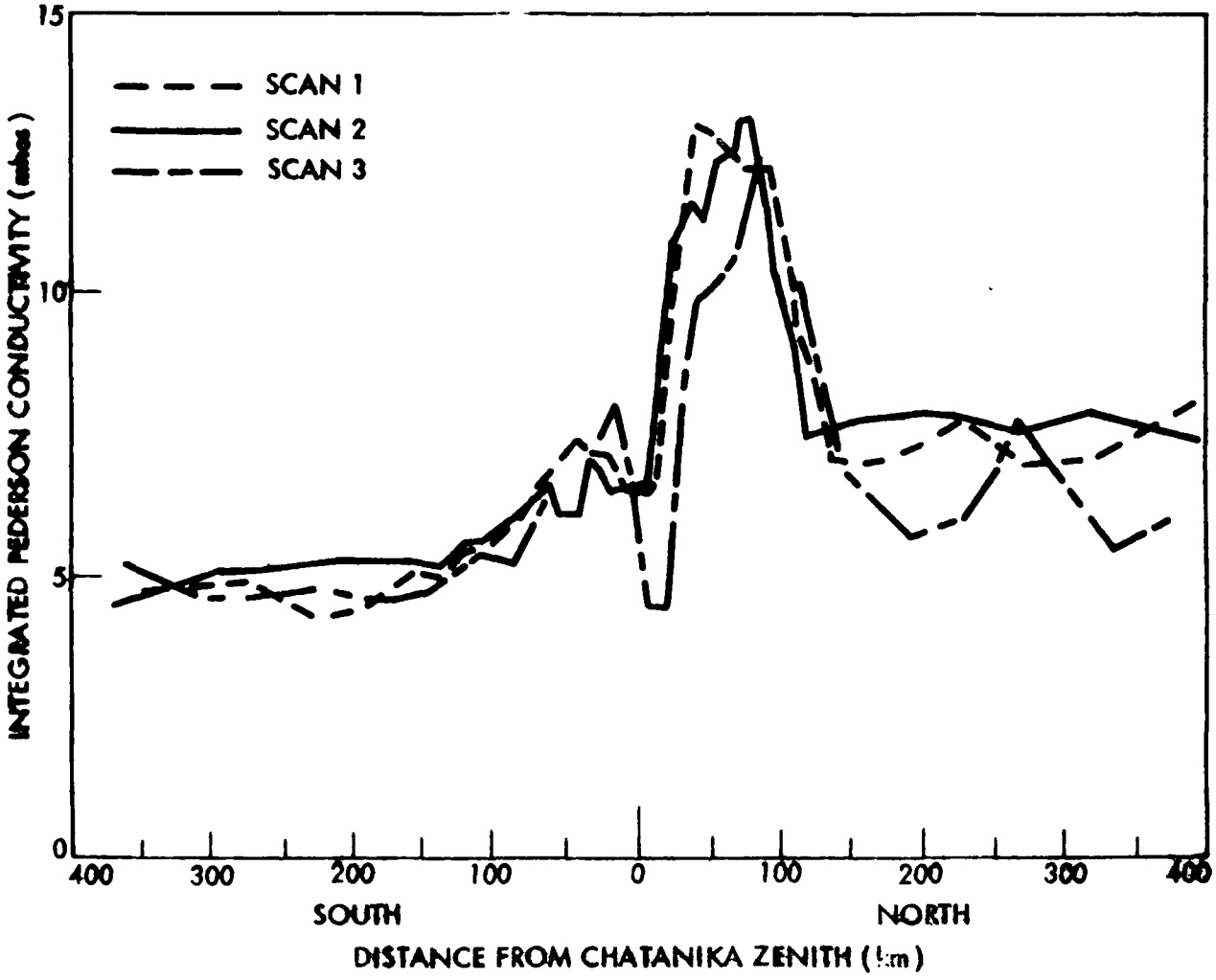

Figure 31. Height-integrated Pederson conductivity for period during SWIR launch, 26 October 1978. Scan times are the same as for Figure 28.

Several features of these data are of interest to the eventual interpretation of the SWIR rocket data; the horizontal width of the arc at half-maximum of the total energy deposit value is approximately 20 km or less most of the time. No other appreciable emission features are located anywhere near the arc during the rocket flight time at least, hence the energy deposit region is very sharply bounded and unique. The mean energy parameter (Figure 29) exhibits similarly well-defined features (as in the classical inverted vee). However, the low level of aurora precipitation to the south of zenith does show some evidence for arclike, inverted vee behavior. This region subsequently developed another arc.

Integrated Hall and Pederson conductivities show somewhat more scatter, but generally appear to reflect the stable, well confined behavior of the ionizing source itself.

3.6 EXCEDE II SUPPORT

The principal photometric support required by EXCEDE II experiments was provided by the three-color meridional scanning photometer. The photometric data were intended to define the location and intensity of possible auroral contamination to the onboard instrumentation. Launch criteria required that any significant auroral activity be located well to the north of the EXCEDE II trajectory. Figure 32 indicates the raw intensity data obtained during the EXCEDE II launch period by the scanning photometer. Because the rocket portion of the experiment failed, no further analyses of these ground-based data were initiated.

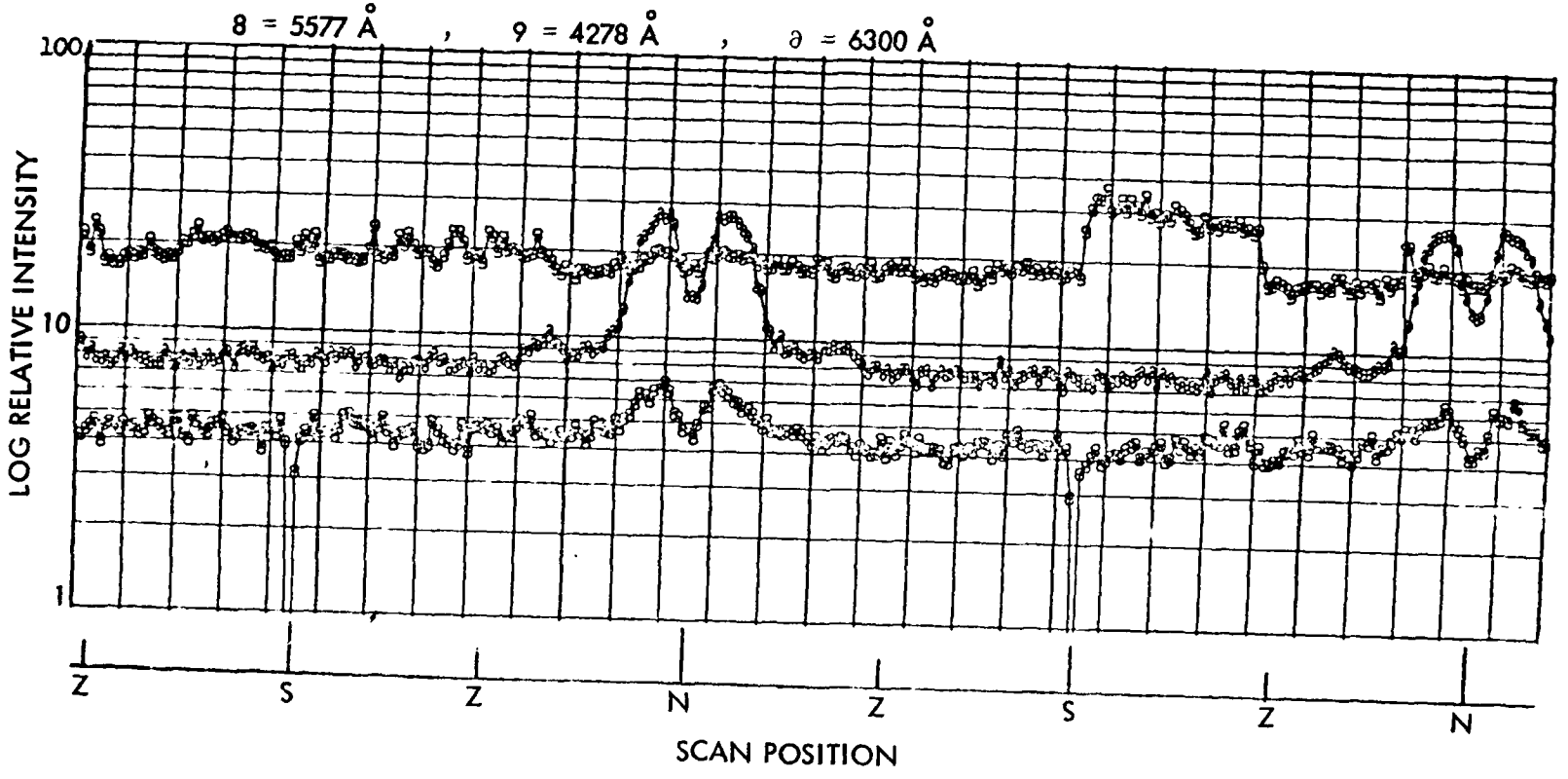

Figure 32. Three-color scanning photometer data for period of EXCEDE launch on 29 October 1978. Data segment extends from 0525:09 through 0530:08UT. Note auroral emission at northern horizon, with no perceptible precipitation elsewhere. Small irregularities observed in channel 9 (427.8 nm) may be due to light scattered from thin haze or clouds.

Section 4
REFERENCES

1. Sears, R. D., Coordinated Measurements of Ionospheric Irregularities: Digital Photometer Design and Development, Topical Report, Contract DASA 01-71-C-0158, LMSC-D311213, 20 Oct 1972

2. Sears, R. D., Definition of Energy Input: Operation ICE CAP, Final Report, Contrac DNA 01-72-C-0134, DNA 2985F, LMSC-D311131, 1 Oct 1972

3. Sears, R. D., Ionospheric Irregularities: Alaska Photometric Measurements, Final Report, Contract DNA 001-73-C-0110, DNA 3235F, 4 Dec 1973

4. Sears, R. D., Evans, J. E., and Varney, R. N., ICE CAP Analysis: Mechanisms for Energy Deposit in the Auroral Ionosphere, Interim Final Report on Contract DNA 001-73-C-0224, DNA 3293F, 15 Jan 1974

5. Sears, R. D., Ionospheric Irregularities: Auroral Motions and Plasma Drifts, Final Report, Contract DNA 01-74-C-0179, DNA 3514, LMSC-D405729, 30 Sep 1974

6. Sears, R. D., ICE CAP Analysis: Energy Deposit and Transport in the Auroral Ionosphere, ICE CAP 73-74, HAES Report No. 5, Final Report DNA 01-73-C-0224, DNA 3566F, 15 Nov 1974

7. Sears, R. D., "Versatile Family of Modular Aurora and Airglow Photometers," Appl. Optics, Vol. 12, 1973, pp. 1349–1355

8. Sears, R. D., "Intensity Correlations of the 4278 Å N_2^+ (0-1) First Negative Band and 5875 Å Emissions in Auroras," J. Geophys. Res., Vol. 80, 1975, pp. 215–217

9. Sears, R. D., and Evans, J. E., Coordinated Optical and Radar Measurements of Auroral Motions and Ionospheric Plasma Drift in Atmospheres of the Earth and Planets, Ed. B. M. McCormac, D. Reidel Pub. Co., 1974

10. Sears, R. D., Ionospheric Irregularities, HAES Program Support, HAES Report No. 29, Final Report, Contract DNA 001-75-C-0098, 30 Sep 1975

11. Sears, R. D., Ionospheric Irregularities: Optical Support of HAES Scintillation Experiments: Final Report, Contract DNA 001-76-C-0182, DNA 4240F, 31 Jan 1977

12. Wickwar, V. B., M. J. Baron, and R. D. Sears, "Auroral Energy Input From Energetic Electrons and Joule Heating at Chatanika," J. Geophys. Res., Vol. 80, 1975, p. 4364

13. Vondrak, R. R., and R. D. Sears, "Comparison of Incoherent Scatter Radar and Photometric Measurements of the Energy Distribution of Auroral Electrons," J. Geophys. Res., in publication, 1978

14. Sears, R. D., and R. R. Vondrak, "Latitudinal Distribution of Ionospheric Conductivity in the Auroral Region," Trans. AGU, EOS, Vol. 58, 1977, p. 1206, Also, Vondrak, R. R., and R. D. Sears, "Comparison of Incoherent Scatter Radar and Photometric Measurements of the Energy Distribution of Auroral Electrons," J. Geophys. Res., Vol. 83, 1978, p. 1665

15. Peterson, A. W., and L. M. Kieffaber, "Airglow Fluctuations at 2.2 μm," J. Atmos. Terr. Phys., Vol. 34, 1972, p. 1357

16. Krassovsky, VI.I., "Infrasonic Variations of OH Emission in Upper Atmosphere," Ann. Geophys., Vol. 28, 1972, p. 739

17. Kumer, J., Further Evaluation of ICE CAP Auroral 4.3 μm Zenith Radiance, Final Report, Contract DNA 001-76-C-0015, 1976

Appendix A

1977–1978 DATA SYNOPSIS SHEETS

SYNOPSIS OF DATA

Tape: OMEGA 1

Date: 11/10/77 **Time:** 0500 - 1125 UT

Photometer(s): 3C(4278, 5577, 6300), 3B1, 3B2

General Activity:

Auroras active in Northern hemisphere of sky all evening.
Bands extended to zenith at times.

Operating Modes:

0630 - 1115	3C, SCAN mode, 10° to 170°, 4° increment, sec dwell
0615 - 1115	3B1, 5577 Å
	3B2, 6300 Å

Notes:

SYNOPSIS OF DATA

Tape: OMEGA 2

Date: 11/11/77 **Time:** 0720 - 1140 UT

Photometer(s): 3C, 3B1, 3B2

General Activity:

Active to north after about 1000 UT

Blowing snow, clear to north, cloudy to south

Operating Modes:

0740 - 1100	3C on scan mode (see OMEGA 1)
	3B1, 5577Å
	3B2, 6300Å

Notes:

Wideband passes covered 0900, 1030 UT

SYNOPSIS OF DATA

Tape: OMEGA 3

Date: 11/12/77 **Time:** 0635 - 1230 UT

Photometer(s): 3C, 3B1, 3B2

General Activity:

Active after about 0800

Operating Modes:

0645 - 1135

3C, scan mode
3B1, 5577 Å
3B2, 6300 Å

Notes:

0940; Wideband pass
0840; Strong arcs near zenith
0955; Eastward surge
1000; In poleward expansion

SYNOPSIS OF DATA

Tape: OMEGA 4

Date: 11/13/77 **Time:** 0830 - 1035 UT

Photometer(s): 3C, 3B1, 3B2

General Activity:

Hazy during entire evening, but auroral structure visible.

Operating Modes:

0850 - 1025 UT	3C, scans
	3B1, 5577 Å
	3B2, 6300 Å

Notes:

0856	FWI rocket launched (0855:00 range time)
1010	Wideband pass covered.

SYNOPSIS OF DATA

Tape: OMEGA 5

Date: 11/17/77 **Time:** 0620 - 1135UT

Photometer(s): 3C, 3B1, 3B2

General Activity:

Very Clear.
Active after about 0830

Operating Modes:

0630 - 1125

3C, scan mode
3B1, 5577Å
3B2, 6300Å

Notes:

1020 Breakup occurs

SYNOPSIS OF DATA

Tape: OMEGA6

Date: 11/19/77 **Time:** 0910 - 1100 0T

Photometer(s) 3C, 3B1, 3B2

General Activity:

Clear

Diffuse activity to north at times

Operating Modes:

0908 - 1054

- 3C, scan mode
- 3B1, 5577Å
- 3B2, 6300Å

Notes:

0910 Wideband pass covered

SYNOPSIS OF DATA

Tape: OMEGA7

Date: 2/27/78 **Time:** 0511-0722 UT

Photometer(s): 3B1, 3Ba, 3C

General Activity:

Active arcs and bands entire period

Operating Modes:

0516 - 0710	3B1, 5577 A
	3B2, 6300 A
	3C scan mode, 10-170°, 4° interval 2 sec dwell time

Notes:

0543 Ba shaped charge

0545 Strong westward surge

0548+ Ba release coincided with very strong auroral enhancement and westward surge. Red lower borders observed

SYNOPSIS OF DATA

Tape: OMEGA8

Date: 2/28/78 **Time:** 0335 -1110 UT

Photometer(s): 3B1, 3B2, 3C

General Activity:

Quiet until 0630 or so

Activity increasing until poleward expansion at ~ 0810

Fairly quiet after about 1030 or so.

Operating Modes:

0400 - 1055	3B1 - 5577 A 3B2 - 6300 A 3C - Scan - standard mode

Notes:

0417 Ba and TMA (Kelley) Rocket launched - quiet conditions

0810 *WIDEBAND-MULTI* Rocket Launched into active arcs near zenith and to north

0929 TRIAD PASS

0952 WIDEBAND Pass

A few problems encountered with voltage to 3CR (channel 10).

SYNOPSIS OF DATA

Tape: OMEGA9

Date: 3/1/78 **Time:** 0430 - 1130 UT

Photometer(s): 3B1, 3B2, 3C

General Activity:

Quiet until 0730, then faint arc thru zenith observed
Faint arc near zenith at 0840
Moderate activity after 0900
Pulsating auroras after 1000 or so.

Operating Modes:

0500 - 1123	3B1, 5890 A
	3B2, 5577 A
	3C Scan Mode - standard (except for times below)
0959 - 1040	3C Up field line, 77° elevation angle

Notes:

0959 - 1011 Special radar - photometer coordination experiment on pulsating auroras
0846 WIDEBAND
0859 TRIAD
1022 S3 - 2 Pass
1031 WIDEBAND Pass

SYNOPSIS OF DATA

Tape: OMEGA10

Date: 3/2/78 **Time:** 0505 - 1237 UT

Photometer(s): 3B1, 3B2, 3C

General Activity:

Active entire night, auroral activity mostly south at late times.

Operating Modes:

0520 - 1110	3B1, 5890 A
1125 - 1237	3B2, 5577 A
	3C, scan, standard mode

Notes:

0926 WIDEBAND Pass

SYNOPSIS OF DATA

Tape: OMEGA11

Date: 3/3/78 Time: 0455 - 1400

Photometer(s): 3B1, 3B2, 3C

General Activity:

Quiet areas to north after 0830 No strong activity - some pulsating forms near zenith after 1200.

Operating Modes:

0640 - 1351	3B1, 5890 A
	3B2, 5577 A
	3C, Scan, standard mode except for times below
0249 - 1300 and 3C, magnetic zenith*	
1320 - 1351	
1300 - 1320	3C, Geographic zenith*

Notes:

*Magnetic zenith and geometric zenith measurements were coordinated experiments with radar and AE-C pass (Fred Rees request).

1310 AE-C Pass

SYNOPSIS OF DATA

Tape: OMEGA 12

Date: 3/4/78 Time: 0547 - 1307 UT

Photometer(s): 3B1, 3B2, 3C

General Activity:

No activity, very hazy skies after 0930.

Operating Modes:

0600 - 1307

- 3B1, 5890 A
- 3B2, 5577 A
- 3C, scan, standard mode

Notes:

0820 WIDEBAND Pass

SYNOPSIS OF DATA

Tape: OMEGA 14

Date: 3/9/78 Time: 0710 - 1200

Photometer(s): 3B1, 3B2, 3C

General Activity:

Activity, mainly to North of zenith until about 1000
Activity passes to South after ~1030 with diffuse forms to north of zenith

Operating Modes:

0735 - 1145

- 3B1, 5890 A
- 3B2, 5577 A
- 3C, Scan, standard mode

Notes:

0813 Rice Rocket Launched
1132 AE-C Pass (F. Rees)
There may be sensitivity problems on 3CR (channel 10) throughout evening.

SYNOPSIS OF DATA

Tape: OMEGA 15

Date: 3/10/78 Time: 0545 - 1215 UT

Photometer(s): 3B1, 3B2, 3C

General Activity:

Active, small substorm near 0800. Diffuse forms over sky after 0800. Intense N-S arc at 1110.

Operating Modes:

0605 - 1201	3B1, 5890 A
	3B2, 5577 A
	3C, scan, standard mode

Notes:

Radar on multipulse all evening. May be a good night to compare neutral winds and E-fields.

SYNOPSIS OF DATA

Tape: OMEGA 16

Date: 3/11/78 Time: 0645 - 1200 UT

Photometer(s): 3B1, 3B2, 3C

General Activity:

Quiet until 0900. Arc to north with breakup after 0930.

Operating Modes:

0655 - 1115

- 3B1, 5890 A
- 3B2, 5577 A
- 3C, standard scan mode

Notes:

Possible problems with 3CR (channel 10) sensitivity.

SYNOPCIS OF DATA

Tape: OMEGA 17

Date: 3/12/78 Time: 0535 - 1140 UT

Photometer(s): 3B1, 3B2, 3C

General Activity:

Quiet and hazy

Operating Modes:

0615 - 1135

- 3B1, 5890 A
- 3B2, 5577 A
- 3C, standard scan mode

Notes:

AD-A085 578 LOCKHEED MISSILES AND SPACE CO INC PALO ALTO CA PALO --ETC F/G 4/1
GROUND-BASED PHOTOMETRIC MEASUREMENTS HAES PROGRAM SUPPORT.(U)
JAN 79 R D SEARS DNA001-77-C-0329

UNCLASSIFIED DNA-4975Z NL

2 of 2

END
DATE FILMED
7-80
DTIC

SYNOPSIS OF DATA

Tape: OMEGA 18

Date: 3/13/78 Time: 0545 - 1340 UT

Photometer(s): 3B1, 3B2, 3C

General Activity:

Moon up early evening.
Hazy most of evening.
Weak to no activity.

Operating Modes:

0615 - 1155

- 3B1, 5890 A
- 3B2, 5577 A
- 3C, standard scan mode

Notes:

3B2N acting up most of evening.

SYNOPSIS OF DATA

Tape: AGINØ1

Date: 10/25/78 **Time:** 0520 to 0840 UT

Photometer(s): 3B1, 3C

General Activity:

None - clouded over by 0700

Operating Modes:

0610 - 0840 3B1 - 5890Å

" " 3C - Standard scan mode
10°- 170° limits, $\Delta L=4^{\circ}$, 2 sec. dwell

Notes:

MTP not run - PM tubes not cold enough.
3C operated on 4278Å, 5577Å, 6300Å

SYNOPSIS OF DATA

Tape: AGIN02

Date: 10/26/78 **Time:** 0430 - 1055 UT

Photometer(s): 3B1, MTP, 3C

General Activity:

0430 - 0800 - Quiet
0800 - Increasing auroral intensity in N.
0848 - Arc at 65° elevation
1030 - Sky very hazy

Operating Modes:

0500 - 1135: 3B1 on 5890Å
MTP on DCR (no filters)
3C on std. scan mode

Notes:

0914 1 SWIR Rocket launched
1 Energy Rocket launched
1 TMA Trail launched-failed
2nd SWIR did not launch
1037 DMSP Pass

SYNOPSIS OF DATA

Tape: AGINØ3

Date: 10/29/78 **Time:** 0425 - 1030 UT

Photometer(s): 3B1, MTP, 3C

General Activity:

0440 - 0640	Very quiet Some Auroral Activity in North, brief duration.
0930	Solid Haze

Operating Modes:

0440 - 1000	3B1, MTP on 7900Å 3C, Std. scan mode

Notes:

0502	EXCEDE Launch
0831	Wideband Pass

SYNOPSIS OF DATA

Tape: AGINØ4

Date: 10/31/78 **Time:** 0800 - 1110 UT

Photometer(s): 3B1, MTP, 3C

General Activity:

0800 - Slight haze
0900 - Weak Aurora to zenith
1100 - Increasing haze

Operating Modes:

0815 - 1100 , 3B1 - 7900Å
MTP - 7900Å
3C - Standard scan mode

Notes:

0950 WIDEBAND Pass
1031 DMSP Pass

SYNOPSIS OF DATA

Tape: AGINØ5

Date: 11/1/78 **Time:** 0420 - 1150 UT

Photometer(s): 3B1, MTP, 3C

General Activity:

0600 - 1130 Active Throughout
~0900 Intense arcs at zenith

Clear all night.

Operating Modes:

0440 - 1135 3B1 - 4278Å
MTP - 4278Å
3C - Standard scan mode.

Notes:

1014 UT DMSP Pass
1030 UT WIDEBAND Pass

SYNOPSIS OF DATA

Tape: AGIN06

Date: 11/2/78 **Time:** 0600 - 1205 UT

Photometer(s): 3B1, MTP, 3C

General Activity:

0800 Hazy, Auroras to north

Variable haze all night
Active most of night.

Operating Modes:

0625 - 1151	3B1 - 5890Å	
	3C - Standard scan mode	
0625 - 1053	MTP - 7900Å	
1053 - 1151	MTP - 4278Å	

Notes:

0925	WIDEBAND Pass
0956	DMSP Pass
1110	WIDEBAND Pass

DISTRIBUTION LIST

DEPARTMENT OF DEFENSE

Assistant to the Secretary of Defense
Atomic Energy
ATTN: Executive Assistant

Defense Advanced Research Project Agency
ATTN: TIO

Defense Nuclear Agency
ATTN: RAAE
4 cy ATTN: TITL

Defense Technical Information Center
12 cy ATTN: DD

Field Command Defense Nuclear Agency
ATTN: FCPR

Field Command
Defense Nuclear Agency
Livermore Division
ATTN: FCPRL

Undersecretary of Defense for Resch. and Engrg.
ATTN: Strat. and Space Systems (OS)

DEPARTMENT OF THE ARMY

Harry Diamond Laboratories
Department of the Army
ATTN: DELHD-N-P

DEPARTMENT OF THE NAVY

Naval Research Laboratories
ATTN: Code 6780, S. Ossakow

Naval Surface Weapons Center
ATTN: Code F31

DEPARTMENT OF THE AIR FORCE

Air Force Geophysics Laboratory
ATTN: OPR, S. Stair
ATTN: OPR, R. Murphy
ATTN: OPR, R. O'Neil
ATTN: OPR, R. Nadile
ATTN: OPR, J. Kennealy

Air Force Weapons Laboratory
Air Force Systems Command
ATTN: SUL

DEPARTMENT OF DEFENSE CONTRACTORS

Aerodyne Research Inc.
ATTN: F. Bien

Berkeley Research Associates
ATTN: J. Workman

DEPARTMENT OF DEFENSE CONTRACTORS (Continued)

General Research Corporation
ATTN: J. Ise, Jr.

HSS, Inc.
ATTN: M. Shuler

Lockheed Missiles and Space Co., Inc.
ATTN: J. Kumer
ATTN: R. Sears
ATTN: B. McCormick

Mission Research Corporation
ATTN: D. Archer
ATTN: F. Fajen
ATTN: R. Hendricks
ATTN: D. Sappenfield
ATTN: R. Kilb
ATTN: R. Stagat

Photometric, Inc.
ATTN: I. Kofsky

Physical Sciences, Inc.
ATTN: G. Calidonia

R & D Associates
ATTN: F. Gilmore
ATTN: C. MacDonald

R & D Associates
ATTN: H. Mitchell

Science Applications, Inc.
ATTN: D. Hamlin

SRI International
ATTN: W. Chesnut
ATTN: C. Rino

Utah State University
ATTN: D. Baker

Utah State University
ATTN: J. Ulwick

Visidyne, Inc.
ATTN: J. Carpenter
ATTN: W. Reidy
ATTN: C. Humphrey
ATTN: H. Smith

General Electric Company-TEMPO
ATTN: T. Stephens
ATTN: DASIAC